Die approbierte Originalversion dieser Diplom-/Masterarbeit ist in der Hauptbibliothek der Technischen Universität Wien aufgestellt und zugänglich.
http://www.ub.tuwien.ac.at

The approved original version of this diploma or master thesis is available at the main library of the Vienna University of Technology.
http://www.ub.tuwien.ac.at/eng

TECHNISCHE UNIVERSITÄT WIEN
Vienna University of Technology

DIPLOMARBEIT

High cycle fatigue properties of Cu films

Ausgeführt am Institut für

Festkörperphysik

der Technischen Universität Wien

unter der Anleitung von

Ao.Univ.Prof. Dipl.-Ing. Dr.techn. Christoph EISENMENGER-SITTNER
Mag. Dr.techn. Golta KHATIBI

durch

Thomas Walter

Arnsteingasse 4/9
A-1150 Wien

Wien, am 26. August 2014

Danksagung

An erster Stelle bedanke ich mich bei meinem Betreuer Prof. Eisenmenger-Sittner für die Unterstützung und die unkomplizierte Ermöglichung dieser Diplomarbeit.

Einem großen Dank bin meiner zweiten wissenschaftlichen Betreuerin Dr. Golta Khatibi, die mit viel Führung und Unterstützung zum Gelingen dieser Diplomarbeit beigetragen hat verpflichtet. Ich bedanke mich bei meinen Kollegen Dr. Agnieszka Betzwar-Kotas, Mag. Bernhard Czerny und Mag. Julien Magnien die mich bei den praktischen Messdurchführungen unterstützt haben und bei der gesamten Arbeitsgruppe "Mikromaterialien" für die angeregten Diskussionen.

Ich bedanke mich bei meinen Kollegen am Kompetenzzentrum Automobil und Industrieelektronik (KAI) zuallererst bei Dipl.-Ing. Josef Fugger, der mir die Möglichkeit an diesem Forschungsprojekt mitzuarbeiten gegeben hat. Insbesondere möchte ich mich bei Dr. Michael Nelhiebel, Dr. Walther Heinz und Dr. Werner Robl (Infineon Regensburg) bedanken, die immer für fruchtbare Diskussionen zur Verfügung standen.

Meiner Freundin Nicole danke ich für die liebevolle Unterstützung und den Rückhalt den sie mir gibt

Zuletzt gilt ein en ganz großer Danke meiner Familie, insbesondere meinen Eltern für die ungebrochene Unterstützung auf meinem Weg.

Contents

1 Introduction **7**

2 Fundamentals **11**

2.1 Thin film structures . . . 11
2.2 Thin film deposition . . . 11
2.3 Diffusion barriers . . . 13
2.4 Stresses in thin films . . . 14
2.4.1 Thermal stresses . . . 15
2.4.2 Wafer curvature measurements . . . 16
2.5 Adhesion measurement of thin films . . . 16
2.5.1 Peel tests . . . 17
2.5.2 Scratch and impression tests . . . 18
2.6 Deformation mechanisms under tensile loading . . . 19
2.6.1 Deformation of a single crystal . . . 19
2.6.2 Deformation of polycrystalline material . . . 19
2.6.3 Deformation mechanisms in small scale materials . . . 20
2.7 Fatigue . . . 23
2.7.1 Thermal fatigue . . . 28
2.7.2 Influence of the environment . . . 31

3 Experimental **32**

3.1 Sample Overview and Preparation . . . 32
3.1.1 Copper films on silicon substrate . . . 32
3.1.2 Free standing copper bars . . . 35
3.2 Experimental techniques . . . 36
3.2.1 Ultrasonic resonance system . . . 36

3.2.2 Optical Microscopy . . . 43
3.2.3 Scanning Electron Microscopy (SEM) . . . 44
3.2.4 Peel-Test . . . 46
3.2.5 Laser Doppler vibrometer . . . 46

4 Results and discussion **53**
4.1 Microstructure . . . 53
4.2 Mechanical properties . . . 56
4.3 Adhesion strength . . . 57
4.4 Fatigue response of copper films on substrate . . . 57
4.4.1 Influence of the diffusion Barrier . . . 57
4.4.2 Influence of the microstructure of the Cu films . . . 59
4.4.3 Cu films of type A . . . 60
4.4.4 Cu films of type B . . . 60
4.4.5 Cu films of Type C . . . 62
4.4.6 Microstructural and dimensional factors influencing the fatigue response of thin films . . . 63
4.4.7 Influence of the chemical composition of the electrolyte and the deposition method . . . 68
4.4.8 Fatigue damage . . . 68
4.5 Free standing Copper bars . . . 76
4.5.1 Fatigue lifetime . . . 76
4.5.2 Fatigue damage . . . 77
4.6 Comparison of free standing Cu bars to Cu films on substrate . . . 82

5 Conclusions **83**
5.1 Outlook . . . 85

6 Bibliography **86**

Abstract

In this study mechanical fatigue behaviour of different types of Cu metallization film stacks (consisting of Si/SiO_2/TiW/Cu) on Si substrates was investigated in the high cycle fatigue regime at room temperature. The influence of thickness, grain size and texture as well as the composition of the diffusion barrier on the deformation behaviour of Cu metallization layers in the thickness range of 5 μm to 20 μm was studied. The samples which consisted of Cu-metallized Si strips were subjected to symmetrical tension - compression fatigue loading by using an ultrasonic resonance fatigue testing systems working at 36 kHz at room temperature. Systematic investigations of surface degradation and fatigue damage in the films showed distinct slip band formation in preferentially oriented grains. Evaluation of fatigue life and the degree of damage was based on the determination of the slip band density as a function of loading cycles as measured by means of optical microscopy. The degree of damage was found to be highly dependent on film thickness, grain orientation and grain size. Moreover it was found that there exists a trend between the adhesion strength of Si/diffusion barrier/Cu and the degree of surface damage during the high frequency fatigue loading (higher adhesion strength of the diffusion barriers to the silicon substrate resulted in a higher degree of surface deformation of the Cu films). This result may be used as a measure for the evaluation of the dynamic adhesion response of thin film stacks on Si substrates. Furthermore, in order to study the effect of constraint on the lifetime and cyclic deformation behaviour of the Cu films, free standing miniaturized bar shaped fatigue specimens were prepared by chemical removal of the silicon substrate. Fatigue life curves (Wöhler curves) were determined by using an ultrasonic fatigue system working at 20 kHz and a special set-up suitable for testing of free standing miniaturized specimens. The comparison of fatigue tests on free standing Cu bars with Cu film

stacks of the same thickness and microstructure showed that cyclic induced plastic deformation is noticeably suppressed in constraint films. Cu bars showed a higher density of deformed grains, with rougher and broader extrusions compared to the features observed in Cu films on a silicon substrate. The fatigue life curve of the free standing Cu bars covered a stress range of 15-25 MPa in the high cycle regime ($>10^6$), while early stages of slip band formation on the surface of Cu metallization on Si was observed first at stress levels in the range of 72 MPa. The results of this study are a contribution to understanding the mechanical fatigue response of constrained metallization films on substrates and provides a new efficient methodology for fatigue studies of thin films on substrates in the very high cycle regime.

Chapter 1

Introduction

Since the earliest applications of microelectronics the demand for smaller and faster components is ever increasing. Thin metallization film stacks which are used for internal and external electrical connections in microelectronic devices cover a broad range of products from power semiconductors to micro-electro-mechanical systems (MEMS). While aluminium was the interconnect material of choice in the beginning of microprocessor development, by using advanced metallization technologies copper has now frequently replaced aluminium in semiconductor components. Cu exhibits superior electrical conductivity, better electromigration resistance as well as higher thermal conductivity. The use of copper also allows further miniaturization of the microelectronic components by using advanced etching techniques. Due to the high diffusivity of copper into the silicon, the application of Cu metallization requires suitable metallic diffusion barriers. Several years of research have been spent for developing effective diffusion barriers with optimized adhesion properties to Cu and the Si substrate. Advanced multilayered Cu interconnects are comprised of thin refractory metal films such as Ti, W, Ta and/or their compounds acting as diffusion barrier layers between Cu and the Si wafer. A typical cross section of Cu thin films stacks used in power semiconductor devices is shown in Fig. 1.1. These multilayered structured are composed of a variety of thin metallic, dielectric and passivation layers with different physical and mechanical properties and thickness ranges.

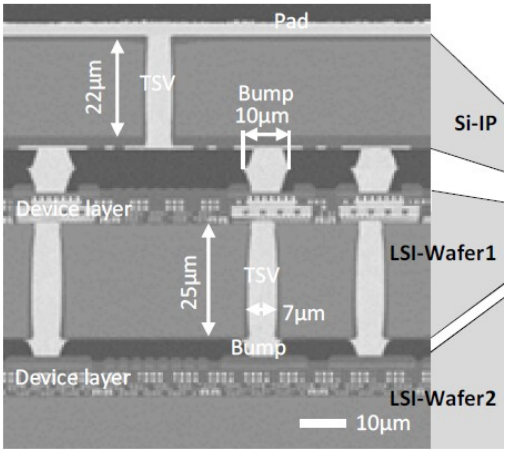

Figure 1.1: SEM micrograph of a multilayer stack (copper bumps/barrier/Si substrate), with interfaces similar to the ones investigated in our study, as an example of usage in modern semiconductor devices [1].

The performance and robustness of thin film stacks depends highly on their electrical, thermal and mechanical properties, the interaction between the neighbouring layers and their response to alternating loading conditions. During the operation thermal fluctuations caused by the electric pulses result in high mechanical stresses between the adjacent layers due to the difference in the thermal expansion coefficient between the metallic film and the substrate. These high stresses may lead to cracking, delamination, and degradation of the metallization and finally result in the functionality loss of the devices. In order to evaluate the reliability of metallization layers a variety of electrical, thermal and mechanical testing procedures are available and are in use for product development or quality control purposes [2, 3]. Since further miniaturization in microelectronic systems is strongly related to advancement of thin film technology detailed knowledge of mechanical properties and fatigue response of thin film stacks and the related degradation and failure mechanisms is of utmost importance. It is well known that mechanical behaviour of small scaled structures with dimensions in the nano- and micrometer range is significantly different to bulk materials [4]. There exists a considerable amount of extensive investigations on the size effect on tensile (flow) behaviour and failure mechanisms of free standing small scaled materials [5, 6]. The cyclic response of scaled materials has not been investigated to such an extent but there

are some elaborate studies on cyclic response of free standing miniaturized samples in which the related deformation mechanisms have been discussed [7]. How far the material properties of free standing miniaturized materials are valid for two dimensional multilayered films stacks is not clear yet. Several studies have shown that constraint materials display other properties than their free standing counterparts [9, 36].

The cyclic response of thin film stacks is rather complex and not only related to their geometrical constraint but factors like the composition of neighbouring layers, processing conditions and internal stresses also play a major role. The main concern during the lifetime of thin film structures seems to be stress induced local deformations, cracking, and delamination of metal layers. A considerable amount of investigations has been performed on the electrical and thermo-mechanical performance of Al metallization films and related failure mechanisms. The thermal fatigue response of Cu film stacks has been studied to some extent; however investigations on their mechanical fatigue response and the related degradation mechanism are scarce. In a study by Zhang et al. [10] on thermal fatigue of thin film copper, a different damage formation mechanism is reported than under uniaxial mechanical cyclic loading. Although the damage mechanisms of thermal fatigue are not fully understood an important factor in the failure mechanisms seems to include grain boundary grooving.

Concerning the fatigue response of thin films on substrates, the focus has been mostly on studying the thermal cyclic response of thin films (below $3\,\mu m$) on Si or flexible substrates [10, 11, 12]. There exist only a few studies on the mechanical fatigue response of Al thin films on Si substrates and systematic studies on mechanical fatigue response of Cu films on Si substrate are not available yet. Mechanical fatigue studies on copper thin films on flexible polyimide substrates were performed by Zhang et al. [10]. The thickness and grain size of the copper film was varied to investigate the influence of the microstructure on the damage morphology, crack initiation and propagation in the strain amplitude range of $8 \cdot 10^{-3}$ and 10^4 cycles. They proposed a model to correlate the observed fatigue damage be-

haviour and dislocation structure with the length scale effect of the thin films. They defined regimes of bulk like behaviour, a transition region and a small volume behaviour depending on the ratio of grain size to film thickness. Larger grains led to extrusions on the surface and well defined dislocation structures. The extrusion width and height increased with increasing the film thickness and crack initiation occurred mainly along these extrusions. The extrusions crossed through the thickness of the film, terminated at the interface with the substrate where void formation was observed [9]. With smaller grains the primary crack initiation sites were found to be at the grain borders. No similar experiments on a rigid substrate have been performed to our knowledge.

The present study concerns the fatigue behaviour of thin Cu metallization films on Si substrates under mechanical cyclic loading in dependency on the microstructure and layer composition. For this purpose an ultrasonic resonance testing system working at 36 kHz was adapted for a specific sample geometry consisting of Si strips with Cu metallization coatings. The selection of the testing system was based on the fact that lifetime data in ultra-high cycle fatigue (UHCF) is increasingly required for development of microelectronic components with design lifetimes of up to 10^9- 10^{10} cycles. In order to fulfil these requirements, an ultrasonic resonance testing system was successfully adapted and employed for fatigue experiments on multilayered thin films on Si substrate. The present work consists of 4 parts. Following the above given introduction, a brief overview of Cu metallization technology and internal stresses in thin films, followed by available thin film characterization methods is given. Further fundamentals of plastic deformation and fatigue of materials is shortly discussed. Chapter 3 includes the experimental details including the description of the sample preparation and characterization methods and the equipment, analytical techniques and the experimental procedures used in this work. The results of fatigue investigations on Cu metallization films as well as free standing Cu bars are given in the last section of this work including data analysis and discussion of the results.

Chapter 2

Fundamentals

2.1 Thin film structures

Thin film stacks can be assumed as two dimensional structures composed of a variety of different materials. The microstructure, especially the grain size, is strongly dependent on the growth parameters such as the deposition technique and the interfaces to the substrate and other neighbouring layers. In the following a short overview on the structure and processing techniques, the state of stress in thin films and their mechanical properties and on fatigue is given.

2.2 Thin film deposition

There are a variety of techniques for thin film deposition, two of which that are relevant to our work, namely sputtering and electrochemical deposition methods, are described below.

Sputtering of thin metal films is widely used because of its low cost compared to chemical vapour deposition (CVD) methods. Common with all sputtering techniques is the physical principle which is the momentum transfer between ionized particles and the atoms of the surface of the target material. The substrate is

placed together with the source material (target) in a vacuum chamber and an inert gas is introduced at low pressure. The gas atoms are ionized by various techniques and accelerated onto the target material. In addition to other processes, target atoms or molecules are sputtered out of the source and transferred and deposited on the substrate. Due to the fact that the underlying principle can be utilised with a wide range of target materials, sputtering is one of the most widespread deposition techniques. A problem to overcome with sputtering techniques is a non-uniform layer deposition when working with non planar topography for examples holes or steps.

Electroplating copper films is a cost effective way to produce copper metallization of more than 5 μm thickness and has been used in the semiconductor industry for some decades. Several problems have to be overcome to receive a smooth and uniform metal layer. Prior to deposition of Cu on the substrate a very thin copper seed layer is sputtered on the barrier films to provide a conductive layer for electroplating the Cu metallization. An electric current is then applied to deposit the copper layer on the device. Alongside the requirement of a uniform current distribution to retrieve a metal layer of uniform thickness additives have to be added to the electrolytes to obtain the desired microstructure and smoothness of the metallization. These additives depend on the requirements of the metallization layer. For copper electroplating organic molecules, the so called suppressor and accelerator are added to the electrolyte. The suppressor inhibits deposition on the edges, which is necessary to obtain a layer of uniform thickness. The accelerator is responsible for grain refining and optimal crystal growth [13]. The surface and microstructure of the barrier/seed layer stack play a significant role on the texture and grain size of the electroplated copper which should be considered besides the adhesion aspect, when choosing the barrier/seed layer stack to retrieve a copper film of the desired microstructure. It is often necessary to make compromises in the microstructure as certain electrical and mechanical properties have diverging requirements. To stabilize the grain size, the thin film copper stacks have to be annealed after deposition. In the case of the present study annealing of the deposited wafers was conducted at 400°C for 30 minutes.

2.3 Diffusion barriers

As already stated in the introduction copper has more and more replaced aluminium and aluminium copper alloys as interconnect material of choice in the past years. The bulk resistivity of Cu is 40 % less than that of Al and electromigration resistance of Cu is also highly superior to Al.
However these essential advantages are accompanied by new problems. Copper diffuses rapidly into Silicon and SiO_2, forming silicides, which can drastically disturb the device performance. The adhesion of copper films on SiO_2 is also lower compared to aluminium.
To avoid both these problems a diffusion barrier between the substrate and the copper film is needed. A passive diffusion barrier which does not react chemically with any of the adjacent layers is ideal for this purpose. The diffusion along grain boundaries and dislocations is significantly faster than the lattice diffusion at low temperatures, therefore an ideal barrier is one that has some or even no boundaries at all. Other functions and prerequisites for a diffusion barrier are:

- The diffusion barrier should be thermodynamically stable under standard operating conditions and not interact with the adjacent layers.
- The density of the diffusion barrier should be close to the bulk density to inhibit the development of dislocations.
- The diffusion barrier should have a good thermal and electrical conductivity.
- The diffusion barrier should exhibit a good adhesion with the substrate and the Cu-film.
- The microstructure of the diffusion barrier should be amorphous at room temperature and after thermal treatment.

Because fulfilling all these requirements is difficult or sometimes even impossible to achieve due to mutual exclusive prerequisites a compromise has to be made to

find the best barrier for each purpose. Generally speaking metals or compounds with high melting temperature are suitable candidates for diffusion barrier material, because they show a smaller amount of grain boundaries. Therefore refractory based materials seem to be the best choice due to the high melting point and good electric conductivity. The most commonly used barriers are binary or ternary barriers based on the refractory metals Ti, Ta, Cr and W.

Binary barriers consist of an intermetallic compound of two refractory metals or of refractory nitrides. A commonly used binary intermetallic barrier is TiW, as it was also already used in Al interconnects.
Using Nitrides in diffusion barriers has the great advantage that the nitrogen can be used to block possible grain boundaries in the barrier, inhibiting the Cu in using these as diffusion paths. A problem that can occur with these binary barriers is, that they can recrystallize at higher temperatures forming again grain boundaries, that one wanted to avoid in the first place. The solution to this problem can be adding a third element to the binary matrix that can inhibit recrystallization processes. A commonly used example of such a ternary diffusion barrier is TiWN [14].

2.4 Stresses in thin films

During the deposition and processing of thin film samples intrinsic stresses will occur in the metal layer. The sources for these intrinsic stresses are mainly differences of the coefficients of thermal expansion of the film and the substrate, different lattice spacing, and recrystallization processes. These misfits and constraints are compensated by the film material through elastic and plastic deformation. Figure 2.1 shows schematically the generation of the residual, in this case tensile, stresses in the thin film during deposition. Due to surface tension forces or misfits accompanying epitaxial growth the growing film initially shrinks relative to the substrate. As the film is finally required to fit to the substrate the film stretches and the substrate will contract. The tensile forces in the film are compensated by compressive forces in the substrate resulting the stack bending concavely upwards [15].

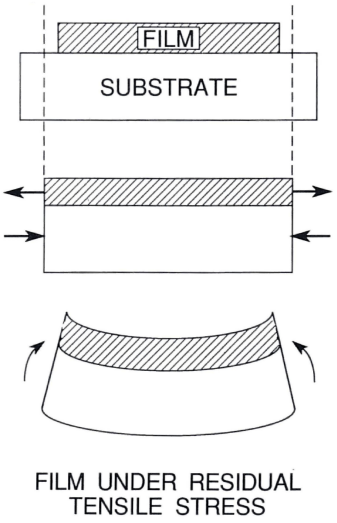

Figure 2.1: Sequence of events leading to residual tensile stress in films [15].

A good approximation for the stress in the film of a film-substrate composite (σ_f) was first published by G.G. Stoney [16] in 1909:

$$\sigma_f = \frac{1}{6R}\frac{E_s d_s^2}{(1-\nu_s)d_f} \tag{2.1}$$

E_s and d_s are the Young's modulus and the thickness of the substrate, d_f the film thickness and R the radius of the curvature. The $1/(1-\nu_s)$ factor is a correction term to account for biaxial stresses. The Stoney formula is useful for determination of film stresses by measuring the bending of thin substrates. The stress increases with larger thickness of the film which was also confirmed on wafer bow experiments performed on the deposited samples as shown in section 2.4.2.

2.4.1 Thermal stresses

Thermal stresses are a further source of residual stress in the deposited films. Thermal stress appears in the film-substrate stack as the deposition process is usually performed at elevated temperatures and the stack is then cooled to room temperature. Using the difference of the thermal expansion coefficients ($\Delta\alpha$) of

the film and the substrate one can calculate the residual stress of an elastically deformed sample by

$$\sigma = \Delta\alpha \cdot \Delta T \cdot E \tag{2.2}$$

where ΔT is the temperature gain and E the Young's modulus.
Wafer bow experiments on the stack samples used in this study showed the tensile stress in the Cu films.
Tensile residual stresses tend to lead to plastic deformation in form of film fracture while compressive stresses can cause wrinkling and local delamination.

2.4.2 Wafer curvature measurements

Wafer curvature experiments are a method to describe the temperature dependent mechanical properties of thin films. The principle of the measurement is based on the change of the curvature of the substrate-film stack of the wafer during the thermal cycling due to the difference between the coefficients of thermal expansion of the film and the substrate. The wafer curvature can be measured by using laser beams or X-ray diffraction methods. The strain in the thin film which is dependent on the thickness of the substrate and the film and their coefficient of thermal expansion can be calculated based on Equation 2.1 [17]. An example of application of wafer bow experiments for stress measurements in thin films used in this work is given in Fig. 2.2. The results show that increasing the thickness of the TiW barriers from 300 nm to 1300 nm leads to reduction of compressive stresses from about 1600 MPa to about 1100 MPa.

2.5 Adhesion measurement of thin films

Measuring adhesion is of great importance for microelectronic components. While fundamental adhesion as a physical phenomenon can hardly be measured or calculated there are several recognized methods to measure practical adhesion and to determine how well a film is bonded to a surface. Adhesion tests can be divided

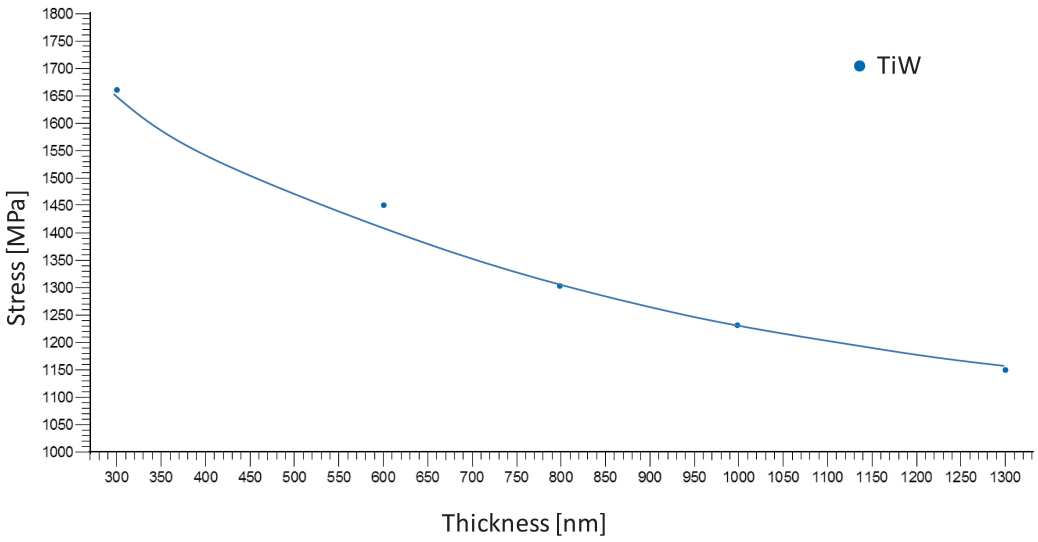

Figure 2.2: Results of a waver curvature measurement of TiW films of different thickness on a silicon substrate. The tensile stress decreases with increasing film thickness.

into two groups, depending whether tensile or shear stresses are generated at the interface during the testing [15, 19].

2.5.1 Peel tests

Peel tests are often used to do a qualitative analysis of the adhesion strength of flexible films. In case of the most commonly used 90 degree peel test the film is fixed with its free end to a loading cell perpendicular to the interface. By moving the loading cell and the interface perpendicular at the same speed, to keep the peel angle fixed, the test can be performed in a steady state condition. The force is measured to determine the bonding strength. Only in special cases the quantitative results of these peel tests can be directly related to the adhesion strength as it would require the film only to deform elastically which is often not the case for thin films. Fig. 2.3 shows schematically the development of the plastic zone in the film during the peel testing.

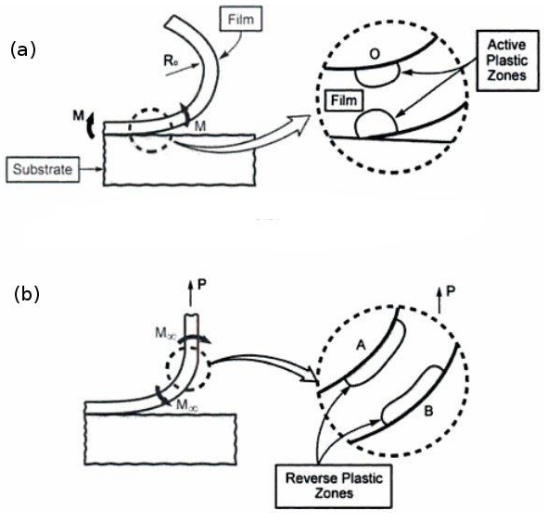

Figure 2.3: Plastic deformation arises in the peeled off layer due to forces during detachment (a) and also forces due to straightening of the film required by the applied loading (b) [19].

2.5.2 Scratch and impression tests

The basic principle of all scratch tests is that a stress induced through indentation results in delamination of the film from the substrate. The tip of a spherical indenter is used to induce a scratch in the film along a certain distance with increasing the load until delamination occurs. Scratch tests have the advantage to work with almost all different kind of film/substrate stacks and also for interfaces that show a strong adhesion. The scratch pattern can be observed by different methods for example by optical or electron microscopy or acoustic detection [20]. The indenter imposes a force to film and the substrate which provides the driving force for separation of the interface. Impression tests are commonly used on brittle coatings with weak adhesion strength to ductile substrates [20].

2.6 Deformation mechanisms under tensile loading

2.6.1 Deformation of a single crystal

When a single crystal is subjected to a certain external load, plastic deformation occurs. The most common way of plastic deformation in crystalline solids is gliding, that is the movement of a dislocation through the crystal. If multiple dislocations glide through the crystal it's called slipping. The preferential orientation for slipping is usually along the closest-packed planes which in the case of face-centred cubic (fcc) crystals such as copper and aluminium are the $\{1,1,1\}$-planes. The direction of the gliding is the direction in the slip plane corresponding to one of the shortest lattice translation vectors which is the $\langle 110 \rangle$ direction for fcc crystals [21]. Face-centred cubic crystals have four $\{1,1,1\}$-planes with three $\langle 110 \rangle$ directions each, and therefore have twelve equivalent slip systems. Depending on the stress and the loading direction only some of them, if any at all are active.
The critical stress and the tensile force required for slip can be calculated by Eq. 2.3 as illustrated in Fig. 2.4. A force F is applied along the axis of the cylindrical single crystal.

$$\tau = \frac{F}{A} cos\phi cos\lambda \tag{2.3}$$

The quantity $cos\phi cos\lambda$ is known as the Schmid factor. Its maximum value is 0.5 when both ϕ and λ are at 45° to the loading direction.

2.6.2 Deformation of polycrystalline material

The deformation of a polycrystalline material is subject to restraints, in such a way that the whole piece of material, with all its differently aligned grains has to be deformed without falling apart. Therefore all grains have to participate in the deformation in a way that each grain influences its neighbouring grains. As explained

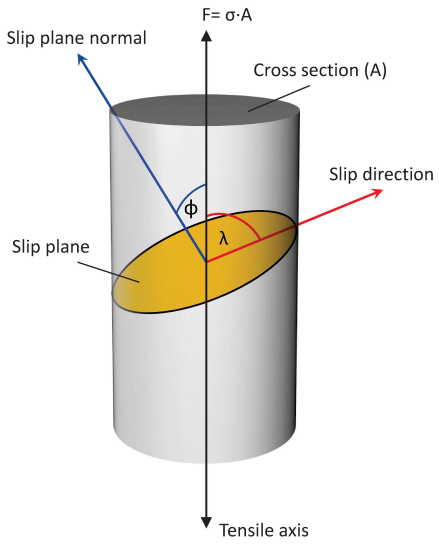

Figure 2.4: Determination of the yield stress depending on the direction of the tensile force in respect to the orientation of a single crystal.

above when applying a load, at first only the grains that are orientated in such a way that they have a slip system with the highest Schmid factor will start to glide. To avoid crumbling of the whole crystal, while the grains exhibit different deformations, geometric dislocations at the grain boundaries are necessary (Figure 2.5).

2.6.3 Deformation mechanisms in small scale materials

In the following paragraphs deformation mechanisms with special attention to dislocation motion as the main source for damage accumulation in small scaled metallic materials is briefly described.

Principally it has been accepted that dislocation motion in thin metal films or small grained materials is inhibited which results to an increase in the yield strength of the material [4]. The strengthening effect due to a decrease in film thickness was first systematically discussed by Nix in [22], where a model of dislocation channelling between two interfaces was proposed and has since then been confirmed by several experiments. The Nix model was later advanced and expanded to include also an effect of the grain size and other strain hardening effect such as

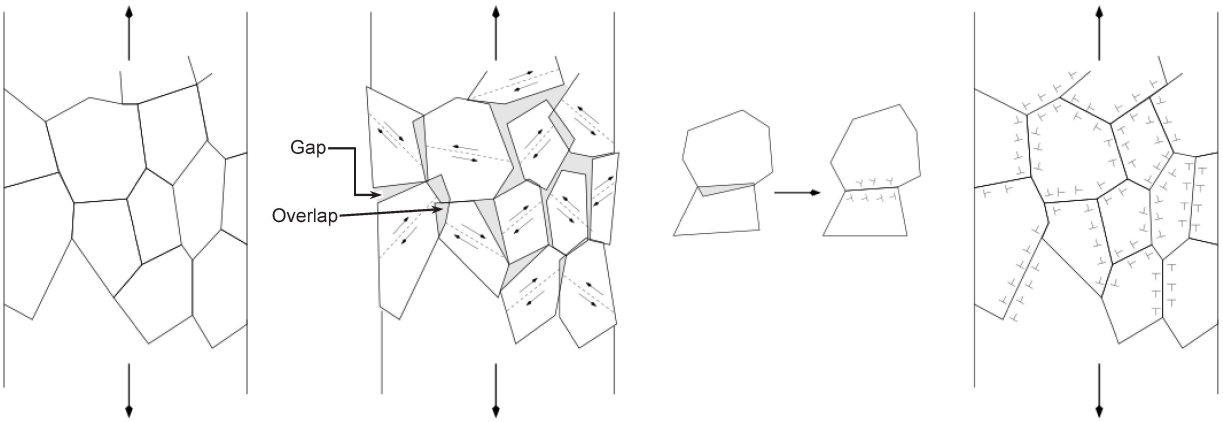

Figure 2.5: Geometrically necessary dislocations prevent a polycrystalline material from decomposing due to the rotation of the single grains under tensile loading.

dislocation pileup against grain boundaries and interfaces. It was shown in several studies that also the ratio of grain size to the film thickness and the film texture strongly influence this strengthening effect.

Mechanical properties of thin films

Several models have been developed to describe the underlying mechanisms that are responsible in the strength increase of thin films on a substrate. An early model by W.D.Nix proposes the so called "threading" dislocations that have their origin in the substrate-film interface and move along the slip planes of the metal grains when an external stress is applied (Fig. 2.6). Thus strain energy is reduced leading to a stress threshold that is decreasing with increasing film thickness necessary for dislocation motion [22].

Grain boundary strengthening

Grain boundary strengthening is a phenomenon of polycrystalline metals. One can find an empirical relation between the yield stress and the grain size of a material, the so called Hall-Petch equation:

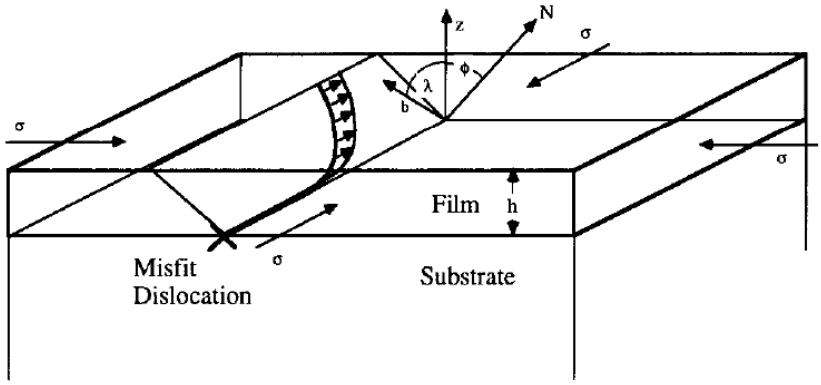

Figure 2.6: Mechanisms for dislocation motion in a thin film on a substrate proposed by W.D.Nix. "Threading dislocations" lead to a dislocation deposition at the interface between film and substrate [22].

$$\sigma = \sigma_0 + \frac{k_y}{\sqrt{D}} \tag{2.4}$$

where σ_0 is the flow stress of an undeformed single crystal and D a measure for the grain size. The additional term can be considered as a strength contribution due the additional resistance to dislocation motion caused by the presence of grain boundaries. There is also an increasing chance that favourable slip directions in one grain may be neighboured to unfavourable slip directions in an adjoining grain. Although experimental results for many materials across a great range of grain sizes show strong conformance with the Hall-Petch relation, the underlying mechanisms may vary.

Another effect that frequently occurs in thin metals films is the strain hardening. The dislocation density increases during plastic deformation. The intersections of dislocations can again inhibit dislocation movement which then leads to an increased yield strength [23].

Thompson [24] proposed a model that includes a threshold for grain size and film thickness and also takes grain orientation into account. The model, which considers grain boundaries as obstacles for dislocation motion was a better model

to describe experimental results than the Nix model or the simple Hall-Petch behaviour.

The influence of a substrate and/or a capping layer on the thin film deformation response has been investigated in [25]. It was found that a substrate also increase the yield strength, due to constraints of dislocation motion at the substrate-film interface. Based on discrete dislocation simulation studies [25] it was concluded that considering the film thickness (d) and grain size (D), the flow stress in thin films is controlled by the smaller dimension between d and D. Furthermore their calculations showed that the stress threshold for "threading" dislocations is about 20 % higher with a rigid substrate than with substrates and capping layers of elastic constants comparable to the metal film.

Influence of the substrate

If a free-standing metal film is subjected to tensile strains it can deform plastically. Experimental results by Xiang [26] showed that for a metal film deposited on a polyimide substrate, due to the geometric constraints from the substrate, the strain localization was suppressed and the film deforms rather uniformly. One can expect to see this constraints effect even enhanced with a rigid silicon substrate, as used in our studies compared to the polyimide substrate in the study mentioned above. It was also shown in this study that the adhesion between the film and the substrate influences these constraints significantly. If the adhesion is poor, local delamination can occur which again leads to localized stress concentrations and crack initiation. The well bonded films could sustain much higher strains than films poorly bonded to the substrate.

2.7 Fatigue

Fatigue is the damage or failure of a material subjected to continuous cyclic loading. Above a certain threshold of the stress or strain applied, microscopic cracks

will appear, preferentially at notches, defects or grain interfaces. The fatigue damage of face-centred cubic (fcc) metals, as used in this study, shows very distinct dislocation structures, surface damage and cracks schematically shown in Fig. 2.7. Under continuous cyclic loading these cracks will grow and the device will eventually fail. The strain that can lead to those cracks can be well below the tensile or yield strengths. Even strains in the elastic range if applied continuously can lead to a change in the microstructure and thereby produce plastic deformations.

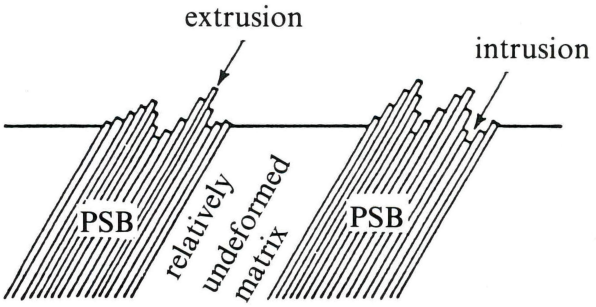

Figure 2.7: A rough surface consisting of hills and valleys produced by plastic strain [18].

In Fig. 2.8 important terms and definitions of a fatigue test are given. The stress amplitude σ_a is defined as $\sigma_a = \sigma_{max} - \sigma_{min}$. The mean stress σ_m (Eq. 2.5) and more often the load ratio R (Eq. 2.6) are common ways to specify the type of the load:

$$\sigma_m = \frac{\sigma_{max} + \sigma_{min}}{2} \tag{2.5}$$

$$R = \frac{\sigma_{max}}{\sigma_{min}} \tag{2.6}$$

$R = -1$ for example means fully reversed cyclic loading, which was the case with all set-ups used for our measurements.

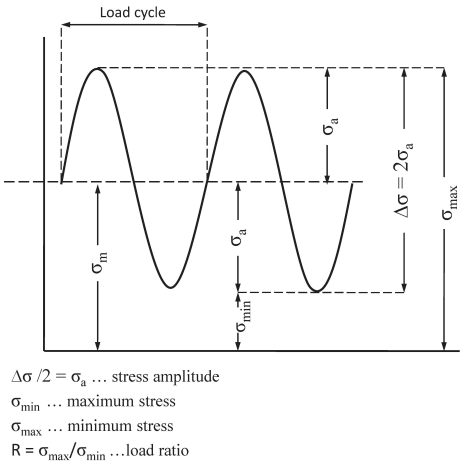

Figure 2.8: Typical cyclic loading parameters in this case for fully tensile cyclic loading ($R > 0$)

There are two different phenomenological approaches to fatigue life, the stress life approach, first introduced by Wöhler in 1860 and the strain life approach proposed by Coffin and Manson independently in 1954.
In the stress life approach the relation of the fatigue life, which is defined as the total number of cycles until failure ($2N_f$) to the stress amplitude can be expressed by the so called Basquin equation [18]:

$$\frac{\Delta\sigma}{2} = \sigma_a = \sigma'_f \cdot (2N_f)^b \tag{2.7}$$

where $\frac{\Delta\sigma}{2}$ is the stress amplitude, σ'_f the fatigue strength coefficient, which correlates with the fracture strength of a material and b the fatigue strength exponent. The latter two being material dependent constants.

In 1954 Coffin and Manson independently found a relation to describe the fatigue life by the strain amplitude in the low cycle fatigue (LCF) range as

$$\frac{\Delta\varepsilon_{pl}}{2} = \varepsilon'_f \cdot (2N_f)^c \tag{2.8}$$

where $\frac{\Delta\varepsilon_{pl}}{2}$ is the plastic strain amplitude, ε'_f the fatigue ductility coefficient, which correlates in monotonic tension to the true fracture ductility and c the fatigue ductility exponent, both being material parameters. $2N_f$ is the number of cycles till failure.

As the total strain is the sum of elastic and plastic strain, in a constant strain amplitude test:

$$\frac{\Delta\varepsilon}{2} = \frac{\Delta\varepsilon_e}{2} + \frac{\Delta\varepsilon_p}{2} \tag{2.9}$$

the Coffin-Manson relationship, Eq. (2.8) provides a practical way to describe the total fatigue life.

If you consider the linear dependency of the elastic portion of the strain with the stress by the Young's modulus (E) to be

$$\frac{\Delta\varepsilon_e}{2} = \frac{\Delta\sigma}{2E} = \frac{\sigma_a}{E} \tag{2.10}$$

the elastic strain can be given by

$$\frac{\Delta\varepsilon}{2} = \frac{\sigma'_f}{E} \cdot (2N_f)^b \tag{2.11}$$

By combining Eqs. (2.7), (2.9) one obtains for the total strain:

$$\frac{\Delta\varepsilon_{pl}}{2} = \frac{\Delta\varepsilon_{el}}{2} + \frac{\Delta\varepsilon_{pl}}{2} = \frac{\sigma'_f}{E} \cdot (2N_f)^b + \varepsilon'_f \cdot (2N_f)^c \tag{2.12}$$

In the low cycle fatigue (LCF) range the fatigue behaviour is predominately governed by the plastic strain. For high cycle fatigue (HCF) the elastic strain becomes the dominant part.

A common way to display fatigue life of materials is a S-N curve, also known as Wöhler curve. The stress amplitude ($\frac{\Delta\sigma}{2}$) is plotted versus the number of load

cycles (N). Usually the number of cycles is plotted in a logarithmic scale. A typical example for an $S-N$ curves for different load ratios (R) of a metallic material are shown in Fig. 2.9.

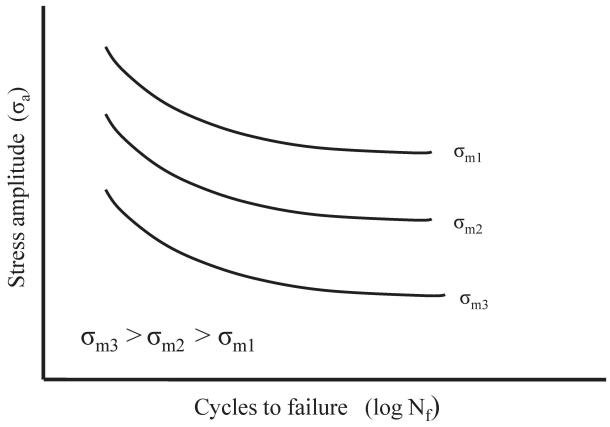

Figure 2.9: S-N curves showing the fatigue life dependency on the mean stress

One can observe that generally a higher mean stress leads to a decreasing fatigue life. This important role of the mean stress has to be taken into account when comparing fatigue results under different loading conditions. There are different theoretical approximations to quantitatively estimate the influence of the mean stress effect on the fatigue life, some of which are plotted in Fig. 2.10. The Gerber relation (Eq. 2.13) has been found to be in good compliance with experimental results of fatigue life of ductile alloys.

$$\sigma_A = \sigma_{fs}(1 - (\frac{\sigma_m}{\sigma_{UTS}})^2) \tag{2.13}$$

The behaviour of materials in the ultra high cycle fatigue (UHCF) regime is still a matter of ongoing discussion. In the early studies it was assumed that Wöhler curves showed a hyperbolic relationship with a horizontal asymptote for the HCF range, which would yield an infinite lifetime below a certain stress threshold. It was later found out, that especially ductile materials such as copper do not seem to have such a conventional fatigue endurance limit. A multi stage S-N curve (Fig. 2.11) was proposed to describe the fatigue behaviour in the UHCF regime [33]. For

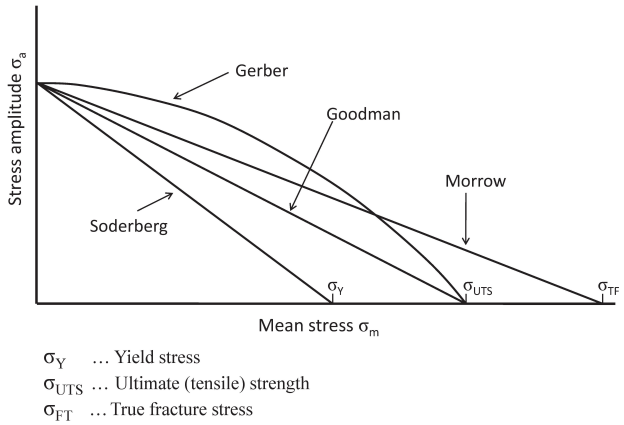

Figure 2.10: Different approximations to estimate the load ratio influence on fatigue experiments

ductile materials like copper at strains below the so called PSB-threshold, where one would not expect to see any more slip bands appear, continuous cycling can lead to surface roughening, because of non-negligible irreversible strain components. These unreversed slip steps will serve as stress concentration factors that increases the localised stress above the PSB-threshold (Fig. 2.12). It is yet unclear at present if there is an actual irreversibility threshold, as shown in Fig. 2.11 and at which stress level it would occur [33].

2.7.1 Thermal fatigue

The main reason for stresses in semiconductor devices is the so called thermal mismatch, that is the difference of the coefficients of thermal expansion of the metal film and the silicon substrate. According to the formula

$$\sigma = \Delta\alpha \cdot \Delta T \cdot E \tag{2.14}$$

one can estimate the stress in the Cu film on the Si substrate with a thermal mismatch $\Delta\alpha = 14 \cdot 10^{-6}$ and a Young's modulus (E) of about 120 GPa during a temperature change of 1°C reasonably well to be in the range of 1.5-2 MPa.

Many of the mechanisms of mechanical fatigue also take place and are compa-

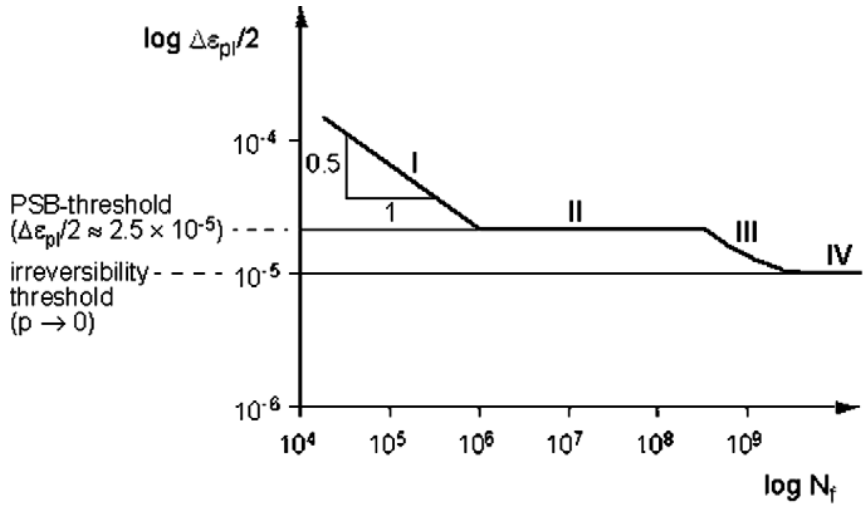

Figure 2.11: Schematic Coffin-Manson type fatigue life diagram for ductile material [33].

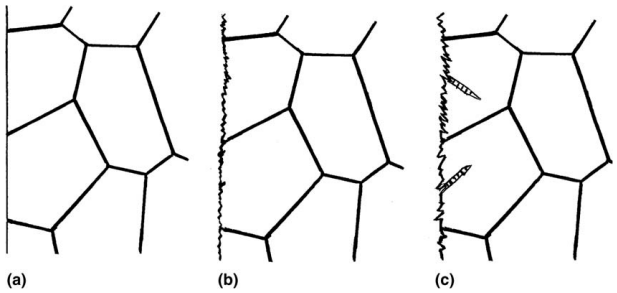

Figure 2.12: Schematic illustration of (a) initial state, (b) early stage of surface roughening and (c) PSB formation at a later stage [33].

rable to thermal fatigue processes as long as temperatures stay below half the melting point. If the maximum temperature is above that limit processes like creep become the dominant part of the deformation. The temperature difference during a thermal cycle is the most important parameter in thermal fatigue, but the mean temperature and also the holding time at the maximum temperature as well as the cycling frequency play a significant role, and makes is hard to compare different results [34].
Generally thermal fatigue experiments are performed in the LCF range, and it is assumed that low cycle thermal fatigue is always somewhere between creep and mechanical fatigue.

The major experimental data on fatigue of thin films is related to thermal cycling experiments on Al and also Cu films as given in the following overview.

All experimental data of fatigue in thin films shows a fatigue response different to that of the bulk material counterpart [8, 10, 11, 27].

Systematic thermal fatigue investigations on 100-300 nm thin Cu films were performed by Mönig et.al [11] with temperature cycles between 100°C and 250°C leading to a total strain range of 0.21 %. They found that with decreasing film thickness the damage mechanisms change from predominantly dislocation glide similar to that in bulk material to a diffusion controlled fatigue damage formation in the very thin films.

TEM investigations of Zhang et al. [10] on thermally fatigued Cu lines with a thickness of 200nm found "parallel glide" dislocations, void formation at twin boundaries and threading dislocations with grain boundaries as main deformation mechanisms.

Heinz et al. [27] performed fatigue experiments on epitaxial Al on (0001) α - Al_2O_3 and polycrystalline Al films on Si substrate. Additionally to the influence of the film thickness they found a strong influence of the texture on the deformation response. Their SEM investigations showed heavy surface deformation caused by dislocation activity and a change in the texture of the thermally cycled polycrystalline 600 nm Al films on the Si substrate. The initial typical $\langle 111 \rangle$ structure for sputtered aluminium changed to a (112) fibre texture. The epitaxial Al showed only a small

increase in surface roughening and orientation of the grains was unaltered even after 10000 thermal cycles. They assumed that interfacial threading dislocations could annihilate each other forming voids at the film substrate interface.

2.7.2 Influence of the environment

Another effect on the fatigue life of the material comes from the environmental conditions. Exposing the material to ambient air, decreases the fatigue life significantly compared to fatigue in vacuum. During the cyclic loading slip steps form and an oxygen layer forms almost immediately on the freshly exposed metal surface. This formation of an oxide makes reverse slip difficult on the same slip plane upon load reversal. This effect becomes amplified at higher temperatures and with increasing humidity of the ambient air [18].

Chapter 3

Experimental

To determine the fatigue behaviour of the thin copper films, free standing copper bars as well as copper films on a rigid silicon substrate were used. Two series of samples were fabricated for this purpose.

3.1 Sample Overview and Preparation

3.1.1 Copper films on silicon substrate

All copper multilayer samples were produced at Infineon Technologies AG in Regensburg on $\langle 100 \rangle$ oriented silicon wafers and had two different basic layer compositions shown in (Fig. 3.1). For preliminary tests on copper films and determining a possible influence of the adhesion on their fatigue behaviour a simpler version of the stack than usually used in semiconductor industry was produced. The samples were prepared in several different steps. On the top of silicon wafers with a thickness of 725 µm a thermal 100 nm SiO_2 layer was grown. On top of this silicon oxide layer a diffusion barrier was deposited by the sputtering technique. Four barriers of different thickness and composition were deposited. An overview of these barriers is given in table 3.1. On top of the barrier a 300 nm Cu seed layer was deposited by sputtering which was then electrochemically grown to form a 20 µm thick copper film. For this first set of samples with the stack I only one kind of electrolyte was

Name	Composition
TiW - #1	300nm TiW (20 wt.% Ti)
TiW - #2	200nm TiW (20 wt.% Ti) + 100nm TiW (29 wt.% Ti)
TiWN - #1	200nm TiW (20 wt.% Ti) + 100nm TiWN (N/Ar=60/100)
TiWN - #2	200nm TiW (20 wt.% Ti) + 100nm TiWN (N/Ar=100/100)

Table 3.1: Overview of the four diffusion barriers of different composition, each of 300nm total thickness that were used for determining the influence of the adhesion on the fatigue behaviour

used for deposition which hereinafter is referred to as type A electrolyte and type A copper respectively. A FIB image of the cross section of one of the stack I samples is given in Fig. 3.3.

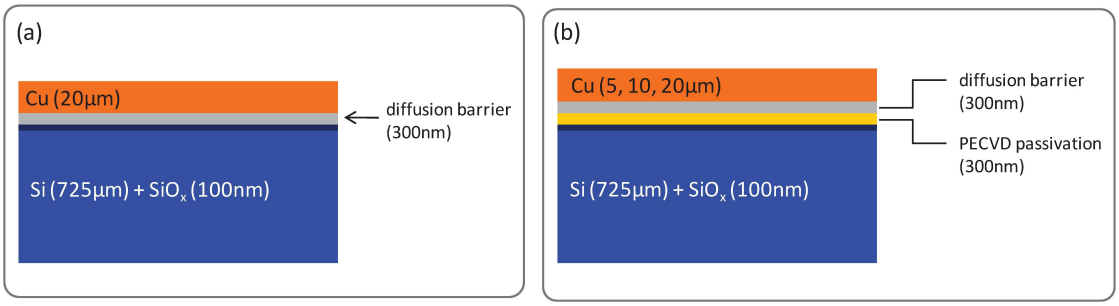

Figure 3.1: Schematic illustration of the Si/SiO_2/barrier/Cu stack stacks used for the fatigue experiments: (a) stack I with 20 µm type A copper only (b) stack II samples were fabricated with three microstructuraly different copper layers of different thickness.

For further tests a stack according to custom and usage in semiconductor components, with additional layers compared to the simpler stack I described above was used. In addition to the thermal oxide layer another SiO_2 layer of 200nm as well as a 300nm thick SiN_x layer were deposited by plasma enhanced chemical vapour deposition (PECVD). A TiW barrier of 300nm such as those used in the stack I was sputtered on top of the silicon nitride. Then the split of three different copper films was deposited on top of the wafers, in each case with two different thicknesses. Besides the type A electrolyte a second electrolyte differing in various organic components hereinafter referred to as type B electrolyte was used. The

third kind of copper film was deposited by the sputtering technique. The different deposition methods and electrolytes led to copper layers of different microstructure that are described in detail in section 4.1. The wafers were then cut with a dicing saw in strips of 10 mm width. The further steps of sample preparation were performed at our own laboratory (section 3.2.1). A complete overview of the samples is given in Figure 3.2.

	Electrolyte (Type A)		Electrolyte (Type B)		sputtered copper (Type C)	
stack I		20µm				
stack II	5µm	20µm	5µm	20µm	5µm	10µm

Figure 3.2: Overview of the different copper layers and stacks used for fatigue experiments

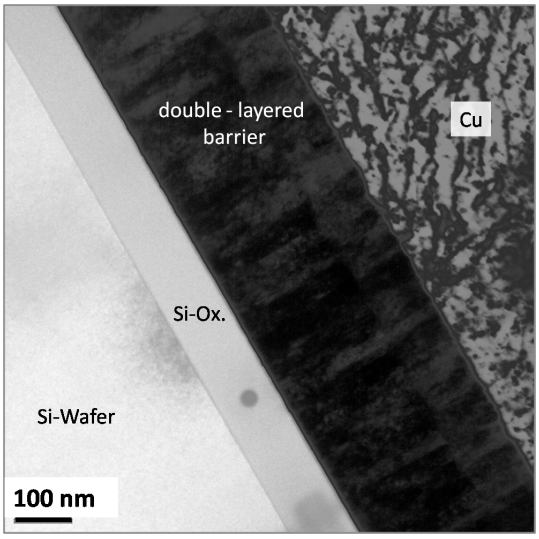

Figure 3.3: SEM image of the cross section of a stack I sample, prepared by FIB technique (image contrast increased to improve interface visibility)

3.1.2 Free standing copper bars

The free standing copper bars were fabricated at Infineon Technologies AG in Regensburg and were initially fabricated in the same way as the thin film samples described above. To retrieve free standing copper bars, the substrate and the diffusion barriers had to be chemically removed.
For this purpose the substrate layers were etched off in a multi step process. First the silicon wafer is wet etched using a 30 % KOH solution at an elevated temperature for several hours. Then the SiO_2 layer and the TiW diffusion barrier were etched using a solution consisting of HF and NH_4 and a solution of H_2O_2 and NH_3 respectively. As a last step the sputtered Cu seed layer was removed using a H_2O_2/H_3PO_4 solution to receive a free standing copper bar of the desired dimension. A more detailed description of the whole process can be found in [5].

In this work Cu-bars with a cross section 20 x 20 µm and gauge lengths of 130 µm were used for the fatigue tests. The samples used to for the fatigue life experiments are shown in Fig. 3.4 and Fig. 3.5. The experimental set-up is described in section 3.2.1.

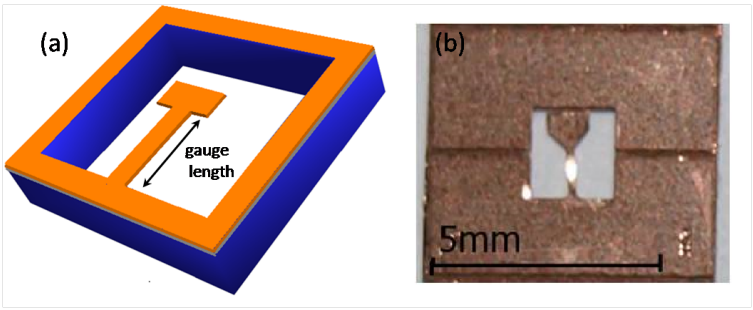

Figure 3.4: (a) Schematic illustration of the Cu bars: The Si/barrier/seed layer stack has been etched off to retrieve a free standing copper bar (b) Free standing copper bar with a width of 200 µm used for preliminary tests.

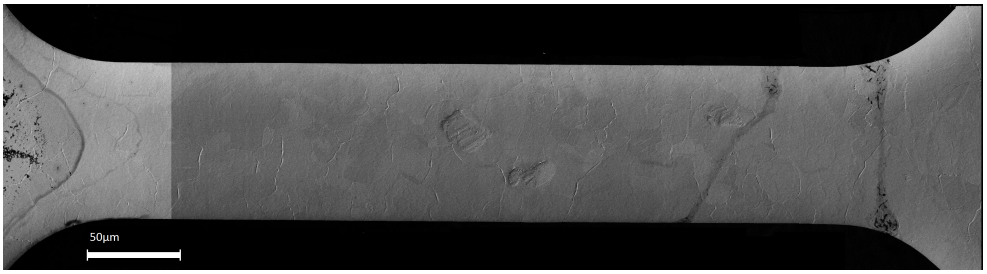

Figure 3.5: SEM image of a free standing Type B copper bar with a width of 80μm before fatigue

3.2 Experimental techniques

3.2.1 Ultrasonic resonance system

Basics

The velocity of a longitudinal wave travelling through a homogeneous solid is:

$$c_{\mathrm{l}} = \sqrt{\frac{E(1-\nu)}{\rho(1+\nu)(1-2\nu)}} \tag{3.1}$$

E being the Young's modulus, ρ the density and ν the Poisson ratio of the material, the latter being a parameter for the contraction perpendicular to the applied load which can be neglected for our experiments yielding a simpler form for Eq. 3.1:

$$c_{\mathrm{l}} = \sqrt{\frac{E}{\rho}} \tag{3.2}$$

Combining this with the simple relation of the velocity c_{l} to the frequency (f) and the wavelength (λ) of the acoustic wave

$$c_{\mathrm{s}} = \lambda f = \lambda \frac{\omega}{2\pi} \tag{3.3}$$

yields a term for the angular frequency of

$$\omega = \frac{2\pi}{\lambda}\sqrt{\frac{E}{\rho}} \tag{3.4}$$

Solving the wave equation, using the boundary conditions of the displacement becoming a maximum at $x = 0$ and $x = L$, yields a term for the displacement amplitude:

$$u(x,t) = u_0 cos(\frac{\pi x}{L}) sin(\omega t) \tag{3.5}$$

As the strain being the derivative of the displacement with respect to the position

$$\frac{\partial u}{\partial x} = \varepsilon(x,t) = -\frac{\pi}{L} u_0 cos(\frac{\pi x}{L}) sin(\omega t) \tag{3.6}$$

one can show that the maximum of this strain function is at $x = \frac{L}{2}$ and that it becomes zero at $x = 0$ and $x = L$. These relations are also shown in Fig. 3.6.

$$L = \frac{\lambda}{2} = \frac{1}{2\nu}\sqrt{\frac{E}{\rho}} \tag{3.7}$$

Set-up

The ultrasonic resonance system for material fatigue consists of a computer controlled ultrasonic-generator that induces the oscillation, which is used to excite a piezoelectric oscillator. The electric oscillation is transformed into mechanical motion. The acoustic wave is then transmitted and amplified through an acoustic horn. The amplification factor mainly depends on the ratio of the cross-section areas on both ends. All the parts, including potential extensions have to be designed in such a way that a standing wave can be exited in the sample or the sample holder respectively. The inherent properties of this set-up lead to a tension-compression load with a stress ratio $R = -1$. The schematic set-up is shown in Fig. 3.6.
The fatigue experiments of the present thesis were accomplished by using two

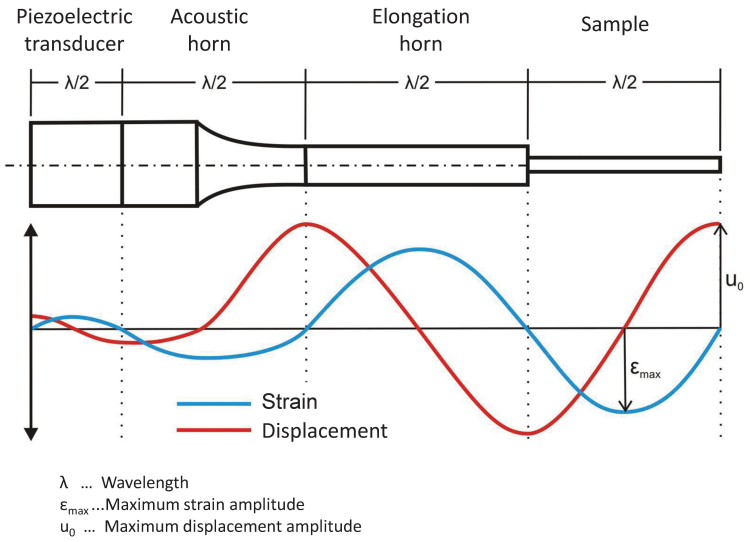

Figure 3.6: Principle of the ultrasonic fatigue testing set-up

ultrasonic resonance fatigue testing systems working at different frequencies of 20 kHz and 36 kHz. The free standing copper bars were fatigued with the 20 kHz system and for the metal layers on the Si substrate a 36 kHz system was used. For further details on the ultrasonic resonance fatigue testing system, refer to [29].

Experimental set-up for fatigue testing of Cu film stacks on Si substrate (36kHz system)

The samples where cut with a glass cutter to a length of 105.7 mm. This length corresponds to the exact length of the Si samples for excitation at a resonant frequency of 36 kHz ($L = \frac{\lambda}{2}$, half wave length) which was determined by calculation using Eq. 3.7. Furthermore finite element (FEM) simulation was used to design the acoustic horn and confirm the calculated specimen dimensions. Using ANSYS software a modal analysis of the specimen oscillation was performed as well to rule out unwanted parasitic oscillations with a frequency near to the desired 36 kHz (see section 3.2.5). Both ends of the Si strips where polished with an abrasive paper to obtain an even surface. To reduce the inherent stresses in the Si strips, resulting from the copper deposition on the silicon wafer, the copper layer was removed from the surface of the Si strips from both ends leaving only a small

copper layer in the middle of the samples symmetrically around the point of maximum strain. The samples where then fitted into the slot of the horn and then glued using a 2-component epoxy glue ("UHU Plus Endfest 300"). The glue was hardened at temperatures of approximately 50-70°C for at least 8 hours which lead to a nominal hardness of the glue of 2000 N/cm^2.

A schematic overview of the 36 kHz system is shown in Fig. 3.7. Strain measurements were performed through direct measurements by using strain gauges (type HBM 1LY11-0.6/120) which were glued onto the backside of the specimen at the site of maximum strain. Additionally displacement measurements were conducted by means of a laser Doppler vibrometer as described in section 3.2.5, which could then be used to calculate the maximum strain.

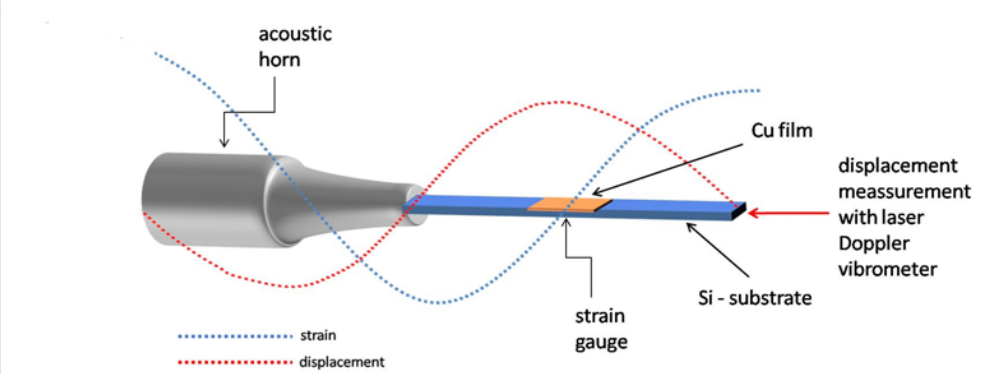

Figure 3.7: A schematic overview of the 36 kHz ultrasonic resonance system set-up by Telsonic that was used to perform the fatigue tests of the Cu films on the silicon substrate

Experimental set-up for fatigue testing of free standing Cu bars (20kHz system)

In order to perform fatigue tests on free standing miniaturized samples a special set-up in combination with an ultrasonic resonance system, working at 20 kHz was used. The samples were mounted over a hole which was introduced in the mid-center of a resonant bar of Ti alloy which was used as a sample holder (Fig. 3.8).

The length of the bar was 125 mm corresponding to the half wave length of titanium at a resonance frequency of 20 kHz, the cross section was 20x8 mm and the diameter of the hole was 1.2 mm. A commercial cyanoacrylate adhesive (Z70 by HBM) was used to glue the samples across the hole in the holder. A similar set-up was already successfully used to measure fatigue properties of thin wires [35] and miniaturized Cu bars prepared by high pressure torsion [32].

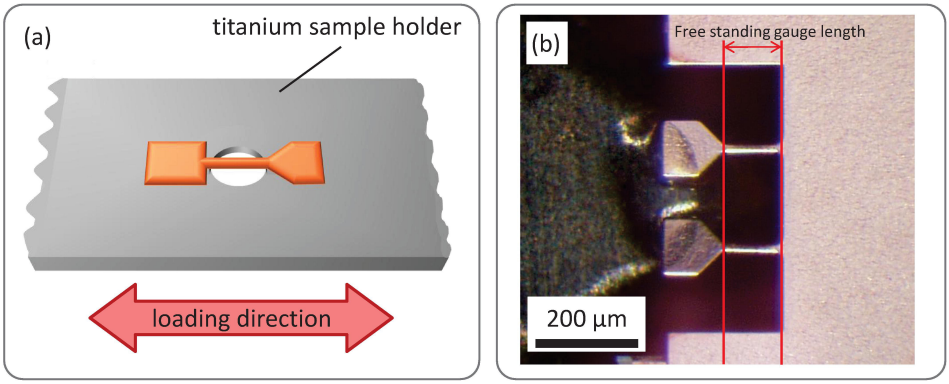

Figure 3.8: (a) Schematic setup of the copper bar mounted across a hole in the centre of a titanium holder; (b) Optical microscope image during fatigue experiments on a pair of type B free standing copper bars with a cross section of 20x20 µm and a gauge length of 130 µm

Calibration of strain

In the present study strain measurements for the free standing copper testing were conducted using strain gauges (type HBM 1-LY11-1.5/120). Strain gauges were glued onto the side of the titanium holder at the location, as well as on the transducer, both at the point of maximum strain. Calibration and measurement of the strain in the free standing Cu bars glued over the notch was performed as below: The stress concentration factor K_t is defined as the ratio of the peak stress (σ_{peak}) due to a notch or an abrupt change in the cross section, to the nominal stress (σ_{nom}) far away from the notch [30]. This is often used in fatigue experiments to reach a certain stress threshold and to increase the stress locally to yield crack initiation at a preferential site. The stress concentration factor can be derived from calculations based on the theory of elasticity, or from stress analysis experiments.

In case of a small circular hole in the centre of a finite width element under uniaxial tension the theoretical stress concentration factor can be calculated using

$$K_t = 2 + 0.284(1 - \frac{d}{H}) - 0.6(1 - \frac{d}{H})^2 + 1.32(1 - \frac{d}{H})^3 \tag{3.8}$$

where d is the diameter of the hole and H the width of the bar [30].
As the theoretical stress concentration factor is only valid for the edge of the hole, the actual stress concentration and therefore the actual strain in the Cu bars had to be experimentally determined. For this purpose Cu bars with a width of about 400 µm were prepared out of the Cu films and glued over the hole. This thickness allowed application of miniaturized strain gauges (type VISHAY FSE-007-12-S6EC) of the film and for direct strain measurements. The calibration measurement was performed using two different transducers over a wide range of amplitudes. The results showed, with all amplitudes a fatigue notch factor (K_f) of 2.35 in comparison with the theoretical stress concentration factor $K_t = 2.83$ calculated using Eq. 3.8 .

Due to the small dimension of the samples in comparison to the titanium holder, fracture of the copper bar has no measurable effect on the oscillation behaviour of the whole resonating system. Thus a frequency shift resulted by cracking and fracture of the bulk samples which is commonly used for failure detection in ultrasonic fatigue systems is not relevant in this case. Therefore the detection of failure of the Cu bars was accomplished by using an optical microscope in combination with a CCD camera during the fatigue testing. The optical set-up was mounted above the sample in order to capture high resolution sequential images from the surface of the Cu bars from which the number of cycles to failure was determined (Fig. 3.9 shows an image of a fractured sample after $1.7 \cdot 10^7$ cycles at a strain amplitude of $2.6 \cdot 10^{-4}$).

The ultrasonic resonance fatigue testing system operating at 20 kHz equipped with a microscope for in-situ deformation (crack growth) measurements is shown in Fig. 3.10.
Since the images of the deformation of the samples during the fatigue testing were

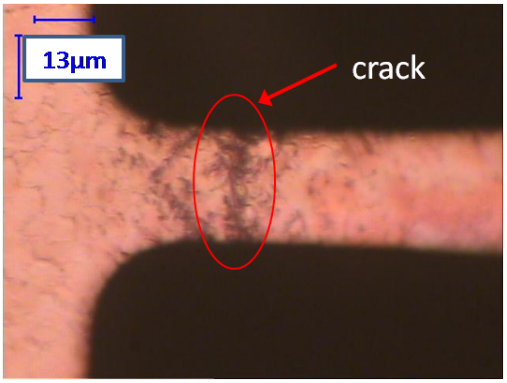

Figure 3.9: Optical microscope image of a ruptured type A free standing copper bar ($N = 1.7 \cdot 10^7$, $\frac{\Delta\varepsilon}{2} = 2.6 \cdot 10^{-4}$)

not taken continuously, the time of fracture was determined within a certain error margin. The minimal interval was set to 5 s resulting in the worst case to an error of well below 1 %. Because the results of fatigue measurements have a high inherent statistical spread, this error can be neglected. Further due to the very limited amount of samples available, only minimal statistical planning and analysis could be performed.

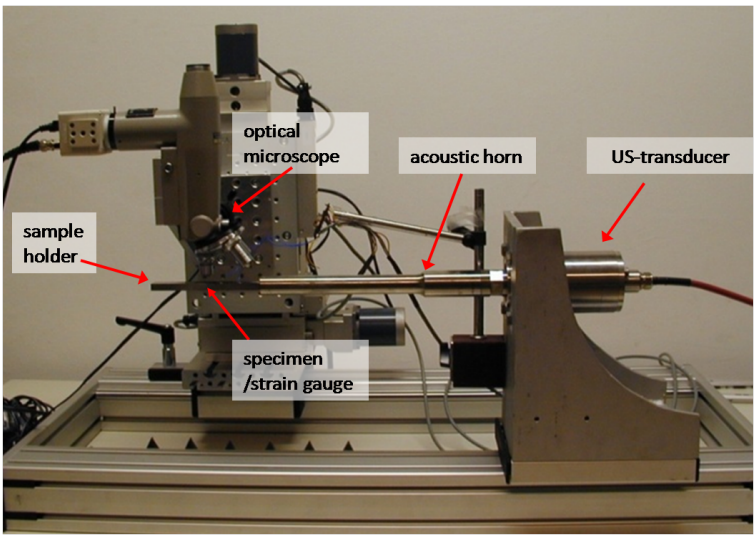

Figure 3.10: The set-up of the 20kHz ultrasonic resonance testing system, used for fatigue experiments on the free standing copper bars

3.2.2 Optical Microscopy

Image Analysis

Conventionally fatigue life is described as the time to fracture of a material. In case of thin films on substrates fracture does not occur in this classical manner and fatigue life can be measured based on the plastic deformation and degradation of the metallic film. Thus in this work the degree of surface deformation was defined as a parameter for the determination of fatigue life which was calculated by using the percentage of deformed area to the whole surface area of the Cu film. The samples were fatigued up to a certain number of loading cycles, the test was stopped and the deformation density was measured. This procedure was repeated several times in certain intervals up to about $2 \cdot 10^9$ loading cycles. For this purpose optical microscope images were used, in which deformed parts of the grains were clearly visible as dark spots. Data analysis was conducted by using the software "Image processing and analysis in java"(ImageJ) [38]. The images were converted to a suitable format and a mask was applied leaving only the spots above a certain grey level threshold visible as can be seen in Fig. 3.11. Manual filtering of the remaining spots had to be performed on each image to ensure that only deformed regions contributed to the total area, as scratches or other damage not caused by the fatigue test could leave similar dark reflections on the images. As the deformed regions vary in size and shape and are hard to distinguish from other damages no automatic filtering script could be applied.
The measured value of the percentage of deformed area to the total area which is called the "deformation density" was then plotted versus the number of loading cycles.

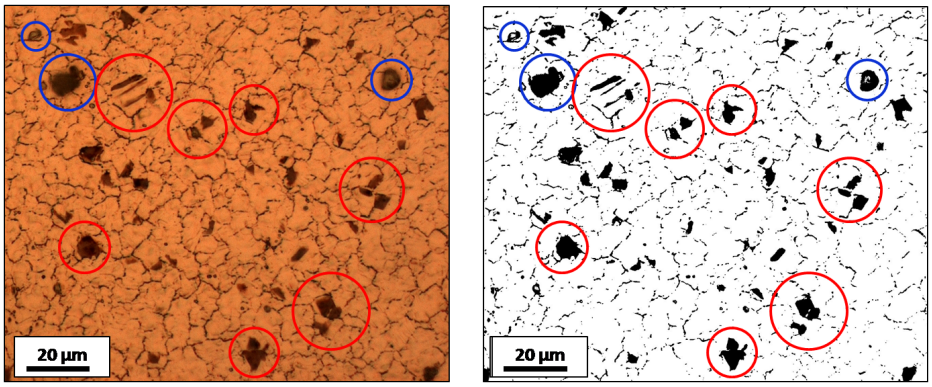

Figure 3.11: (a) Optical microscopy image of the fatigued copper surface(type B copper, stack II after $1.5 \cdot 10^9$ cycles) (b) after pre-filtering the area of the dark spots (deformations) using "ImageJ" software. Manual filtering had to be performed so that damage not caused by fatigue (e.g. scratches), contamination or grain borders (all marked here with blue circles) did not contribute to the deformation density (red circles mark some of the fatigue damage). The images shown here are only a detail of the total area used to determine the deformed area.

3.2.3 Scanning Electron Microscopy (SEM)

SEM-images were used to determine the type and degree of the surface deformation, as well as to determine the microstructure of the material before and after fatigue tests.

Electron channelling contrast imaging was performed on electropolished samples to visualize and investigate the microstructural details such as dislocation structures and twin boundaries within the grains.

Also electron backscatter diffraction (EBSD) maps were recorded to evaluate the texture and grain size of the undeformed and deformed samples and to determine the orientation of the deformed grains.

In our case all SEM investigations were performed on a field-emission SEM (Zeiss Supra 55 VP), which was equipped with an EBSD and EDX detector by Oxford Instruments.

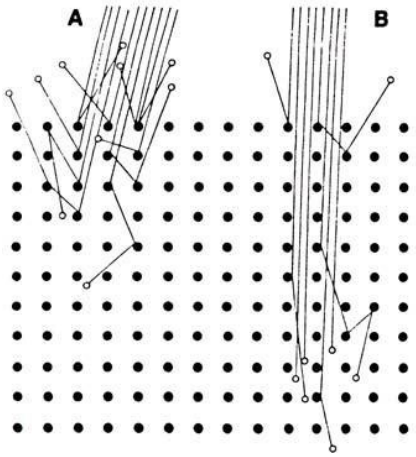

Figure 3.12: Principle of channelling contrast imagery. The yield of reflected particles depends on the orientation of the crytsall latice in respect to the incident beam.

Electron channelling contrast imaging (ECCI)

With the use of the back scatter detector a so called channelling contrast image can be recorded. The intensity of the back scattered electrons depends on the angle between the beam and the lattice planes. A low angle allows the electrons travel deeper into the material along the lattice "channels" resulting in a lower intensity of the elastically scattered electrons as shown in Fig. 3.12. The channelling contrast can be used to distinguish differently orientated grains, lattice defects and subgrain boundaries. To gain viable results the specimen surface had to be electropolished. For this purpose an electrolyte consisting of ethanol and phosphoric acid was used.

Electron backscatter diffraction (EBSD)

EBSD mapping is a technique for obtaining the crystallographic information using the scanning electron microscope. The sample is put in the chamber at a highly tilted angle to the incident beam. The electrons scattered by the atoms in the crystal lattice undergoing constructive or destructive interference as given by Braggs law:

$$2d \sin\theta = n\lambda \tag{3.9}$$

where d is the interplanar distance, θ the scattering angle and lambda the wavelength of the electrons. This leads to a distinctive diffraction pattern dependant on the crystal structure and orientation. An electron backscatter diffraction pattern (EBSP) is formed when many different planes diffract different electrons to form Kikuchi bands which correspond to each of the lattice diffracting planes. By knowing the crystal structure of the material the orientation of the individual grains can be calculated from the Kikuchi bands.
All EBSD measurements were performed by tilting the sample holder by 70°, using a working distance of 9.5 mm and an accelerating voltage of 20 kV. Different step sizes from 100-300 nm were used to scan the Cu surface.

3.2.4 Peel-Test

A simple 90° peel test was performed to determine differences in the adhesion of the different diffusion barriers of the multi-layered copper samples. The sample was mounted with the silicon side onto an x-stage that was moveable horizontally. The Cu/barrier film was partially peeled off and fixed to the grips of a tensile machine which was set up perpendicular to the moveable stage. During the peel testing, the Cu film was subjected to a tensile load while the stage moved simultaneously in the x - direction a way that the force applied to the Cu/barrier interface was 90° at all times. A simple diagram of this basic principle is given in Fig. 3.13, the set-up is shown in Fig. 3.14.

3.2.5 Laser Doppler vibrometer

Non-contact vibrational analysis of the samples was performed by using a laser scanning vibrometer (LSV) and the displacement measurements were conducted by means of a laser Doppler Vibrometer (LDV). The principle of a laser vibrometer

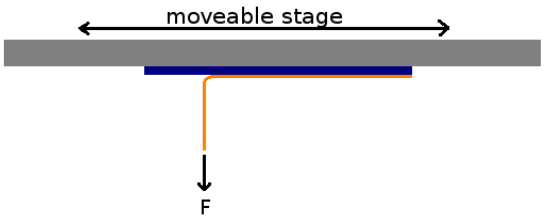

Figure 3.13: Schematics of the 90° peel test for adhesion measurement

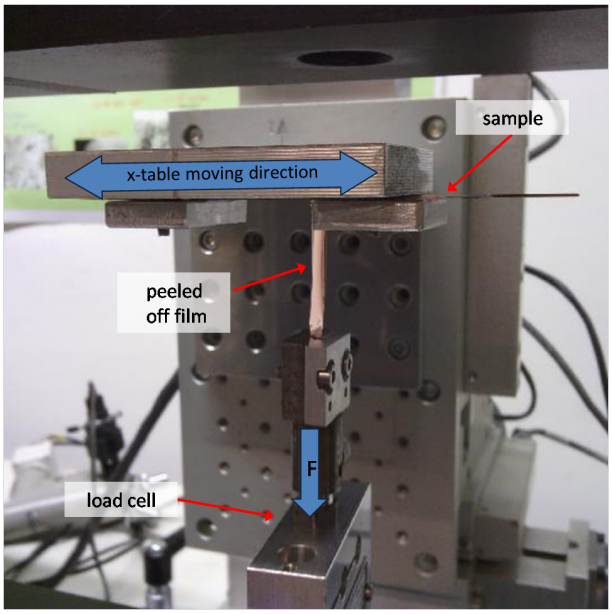

Figure 3.14: Set-up of the 90° peel test

is based on the shift of the frequency of the reflected laser beam in consequence of the Doppler effect and is shown in Fig. 3.15. The velocity of the oscillation can be experimentally determined and thereby the displacement can be calculated. As already derived in Eq. 3.6 the strain can easily be calculated from the displacement of the sample.

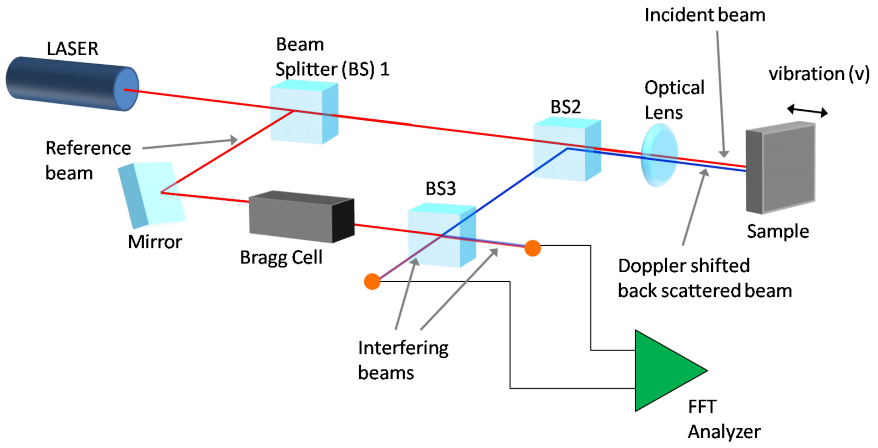

Figure 3.15: Principle of a Laser Doppler vibrometer. The frequency shift of the reference beam and the back scattered beam can be used to calculate the velocity, and the displacement of the oscillation.

To investigate the vibration characteristics, especially oscillation modes that are perpendicular to the induced longitudinal mode, a scanning vibrometer (type PSV-A-410 by Polytech) was used (Fig. 3.16). The physical principle is the same as with the laser Doppler vibrometer. The scanning vibrometer scans multiple arbitrary measuring points on the surface of the sample and calculates the velocity, displacement and phase relations. With this data the oscillation can be visualized [39].

Oscillation analysis

As previously mentioned the residual stresses in the metallized Si sample strips were reduced by removal of the Cu film from the surface except of 5 mm - 20 mm in the middle of the Si samples. However due to an asymmetric sample configuration (the Cu film was deposited on one side of the wafer only) and the geometry

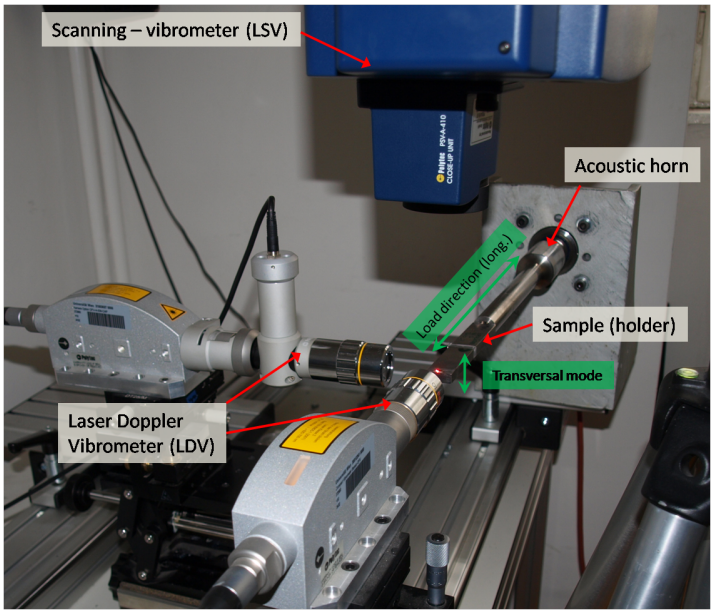

Figure 3.16: Set-up of the Scanning vibrometer/Laser Doppler vibrometer measurements specimen on a titanium sample holder.

(thin Si substrate), by excitation of the longitudinal oscillation mode in the sample an additional transversal mode with a very low amplitude was also induced. This transversal mode which could be detected using a scanning vibrometer influenced the occurrence and distribution of the damage significantly. Fig. 3.17 shows such a transversal oscillation mode in one of the stack I samples where the copper was partially peeled off leaving only a 20 mm Cu strip in the middle of the sample. One can see several peaks indicating a shorter wavelength of the transversal mode compared to the longitudinal mode with one maximum superimposing the longitudinal strain maximum. The transversal displacement is only approximately 9 % of the longitudinal displacement, but still has a clear influence on the surface deformation. According to the sinusoidal displacement/strain distribution in a resonance bar excited to longitudinal mode the strain amplitude gradually drops from the midsection of the sample to the both ends. Thus in case of the present experiments the strain distribution in the form of a half wave would result in a gradual drop of the number of deformed grains from the maximum to the end of the sample. However the deformation density on Cu films shows a peak at the point of maximum strain of the longitudinal mode that drops strongly towards the both endings of the

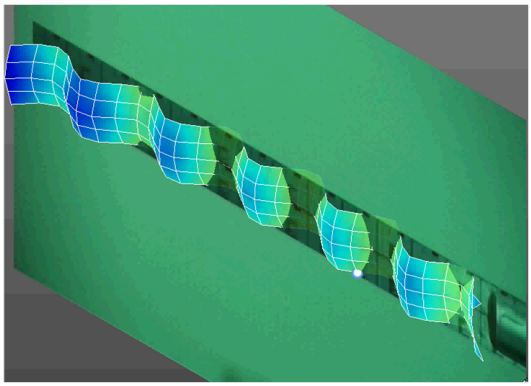

Figure 3.17: Visualization of the transversal mode, using a scanning vibrometer

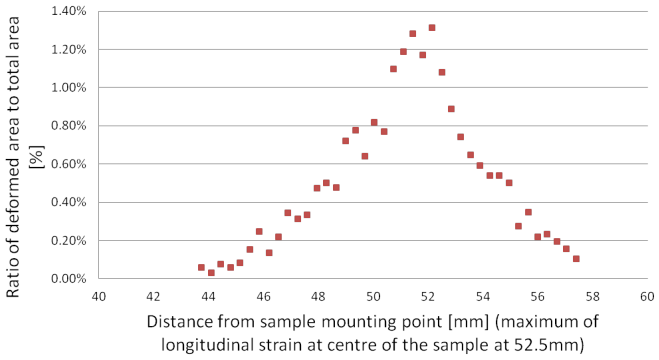

Figure 3.18: The sharp peak of the deformation density distribution at the site of maximum strain indicates superposition of a longitudinal and transversal oscillation mode

sample, deviating from the sinus shape as shown in Fig. 3.17. Therefore it can be concluded that the sharp peak in the damage distribution results from the superposition of the transversal and longitudinal mode, raising the strain above the necessary threshold to induce plastic deformation in the film.

For fatigue tests on the stack II samples the length of the copper coating was further decreased leaving only 5 mm in the middle of the sample. This was done to reduce the transversal mode as far as possible. Scanning vibrometer measurements on these samples showed transversal displacement peaks reduced to less than 1 % of the longitudinal mode. The results are summarized in table 3.2. Deformation distribution suggested that with this fatigue tests, the transversal mode

plays only a negligible role for damage formation.

Specimen	Δu_{long}	Δu_{trans}
stack I (20 mm copper strip)	19.8 µm	1.8 µm
stack II (5 mm copper strip)	20.4 µm	0.16 µm

Table 3.2: Displacement measurements performed by LDV/LSV analysis showed a transversal oscillation with nearly 10 % of the transversal amplitude on the stack I samples. Reducing the Cu strip from 20 mm to 5 mm with the stack II samples reduced this amplitude to less than 1 % of the longitudinal mode

Finite element (FEM) simulation

Fig 3.19 and 3.20 show the displacement plot visualized by FEM modal analysis of the longitudinal and transversal waves in the Si strip sample with one fixed end. They are in good accordance with the vibrometry measurements. The displacement values of this modal analysis, which are directly proportional to the experimental results, predict the transversal displacement at the site of maximum strain to be in the range of 1 % of the longitudinal displacement. The asymmetric displacement distribution for the transversal mode results from the boundary conditions of a completely fixed end of the Si strip of the FEM simulation deviating from the real experimental conditions.

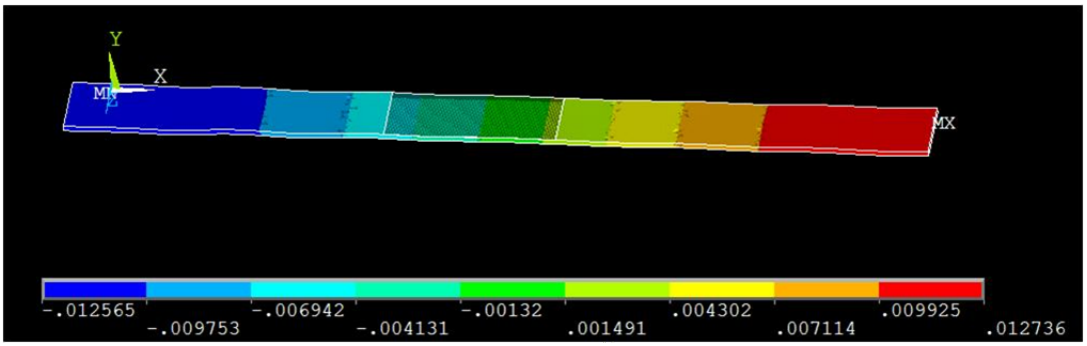

Figure 3.19: FEM simulation (modal analysis) of the longitudinal displacement of a Si strip fixed on one end.

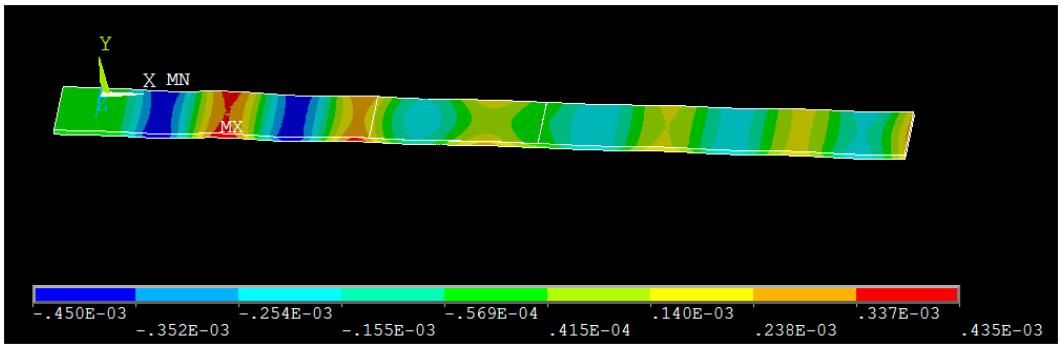

Figure 3.20: FEM simulation (modal analysis) of the transversal displacement of a Si strip fixed on one end.

Chapter 4

Results and discussion

In this chapter the results of the investigation on high cycle fatigue behaviour of Cu thin films are presented. The results include microstructural characterization of the Cu films, the mechanical properties of free standing Cu bars as well as the adhesion strength of the Cu films to Si substrate followed by detailed fatigue investigations and lifetime curves of both types of samples. The experimental results have been discussed and analysed with respect to the state of the art in literature and to our own findings.

4.1 Microstructure

A typical microstructure of the Cu films used in this study is presented in the SEM-ECCI image in Fig. 4.1 which was obtained after electrochemical polishing of the samples. The films showed a rather high percentage of $\Sigma 3$ "Coincident Site Lattice" boundaries that are often found in annealed fcc materials. These crystal twins are rotated 60° about the $\langle 111 \rangle$ direction. The gray shades are related to the different grain orientation of the films as determined by EBSD analysis while the dark spots are artefacts from the electro polishing performed prior to the SEM investigations (see section 3.2.3).

To measure the grain size and texture EBSD imaging and analysis was performed as described in section 3.2.3. The critical misorientation angle defining a grain

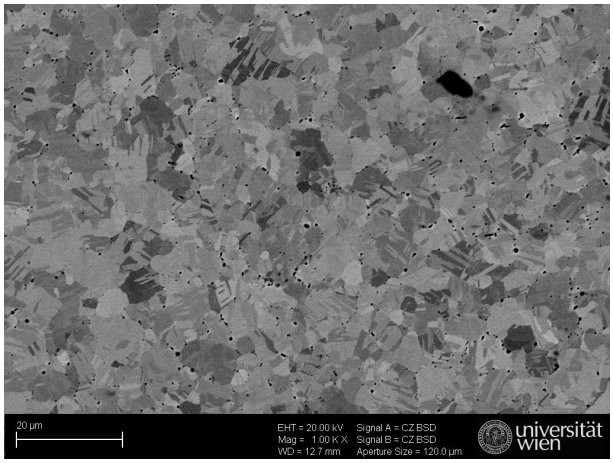

Figure 4.1: SEM-EECI image of a type A - stack I sample.

boundary was assumed to be 5 degree. Twin boundaries of the cubic crystal lattice were disregarded. The grain size in this study is defined as the diameter of a circular grain with an equivalent area to the measured grain which was determined by a suitable software. The investigation showed the following results:

The average grain size of type A copper showed an insignificant dependence on the film thickness. An average grain size of 2.4 µm $\pm$ 1 µm was measured for the 5 µm film while the 20 µm film showed a grain size of 2.9 µm $\pm$ 1 µm.

The grain size increased considerably from 4.0 µm for the 5 µm film to 18.2 µm $\pm$ 6.3 µm for the 20 µm film. A significant number of twin boundaries could be found for the type B copper films as well.

The type C copper layer again did not show a significant thickness dependence on the grain size. The 5 µm and 10 µm films showed a grain size of 2.6 µm and 2.8 µm respectively.

Fig. 4.2 shows the inverse pole figure (IPF) maps of the three types of copper surfaces of different thickness. One can easily see that, while there is a large increase in the grain size of type B copper when the film thickness is increased, the grain size of the type A and type C copper does not change significantly when

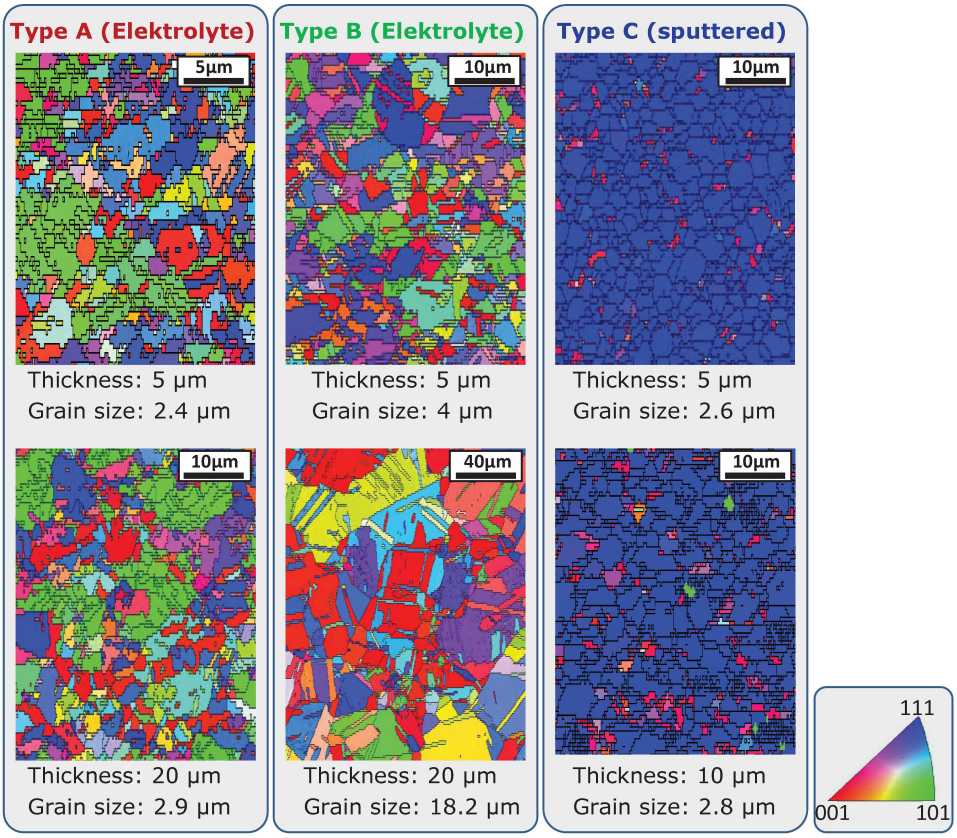

Figure 4.2: EBSD images of the microstructure of the three different copper layers, deposited with electrolyte A and B and by sputtering (Type C) respectively.

varying the thickness.

The same EBSD images were used to determine the texture of the various copper layers. Fig. 4.3 shows the inverse pole figures (IPF) calculated from the EBSD data of the three different types of copper layers with a thickness of 5 µm in the initial state. It can be seen that both, electrodeposited type A and type B copper, exhibit a rather uniform orientation distribution but the Type C sputtered copper displays a strong $\langle 111 \rangle$ out of plane orientation. This is true for both, the thin (5 µm) and the thick (10 µm and 20 µm) films, respectively.

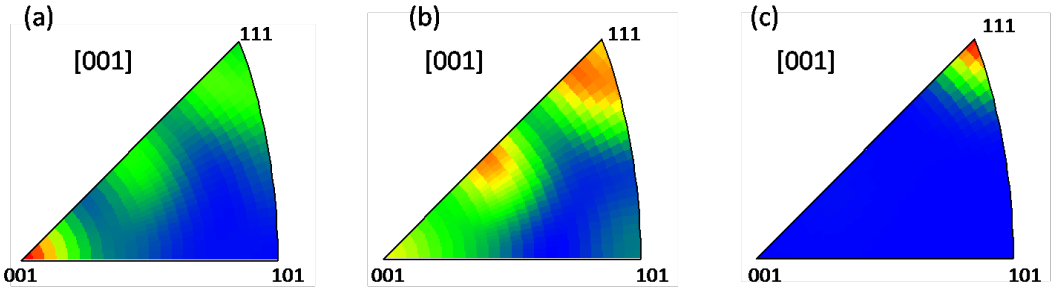

Figure 4.3: Inverse pole figures (IPF)of the three different copper layers a) Type A and b)Type B show rather a uniform orientation distribution while c) Type C shows a distinct $\langle 111 \rangle$ out of plane preferential orientation

4.2 Mechanical properties

The average grain size of the Cu films and the mechanical properties of the respective free standing Cu bars (type A and B) with a thickness of 20 µm are summarized in table 4.1. The ultimate tensile strength (UTS), Young's modulus (E), yield strength ($R_{p,0.2}$) and elongation to fracture ($\varepsilon_{failure}$) were determined by tension tests on the free standing copper bars at the Erich Schmid Institute Leoben [6]. One can see that the type A copper layer shows a significantly higher ultimate tensile strength, yield strength and Young's modulus than the type B copper. Primarily the smaller grain size of the type A copper seems to be responsible for the improved mechanical properties of the films. The finer grains size is related to the applied electrolyte type resulting in a higher impurity concentration. The values of Young's Modulus as given in the table 4.1 are calculated based the EBSD measurement on single grains across the gauge length of Cu bars with a thickness of 20 µm. The lower Young's modulus given for the type B copper is not an average value but corresponds the grains with soft [100] orientation.

Using the SEM, electron channelling contrast images of the copper surfaces were taken to further investigate the grain structure of the Cu-films. As can be seen in Fig. 4.1 a high density of twin boundaries can be found in the Cu-crystals.

Material	Grain size [µm]	UTS [MPa]	E [GPa]	$R_{p,0.2}$ [MPa]	$\varepsilon_{failure}$
Type A	2.8 ± 1.2	291 ± 5	100 ± 15	146 ± 7	0.46 ± 0.05
Type B	22.4 ± 6.3	177 ± 15	70 ± 20	60 ± 12	0.39 ± 0.02
Type C	5 ± 3	–	–	–	–

Table 4.1: Mechanical properties of the stack II samples

4.3 Adhesion strength

To determine the adhesion of the metallization on the substrate peel tests according to the method described in section 3.2.4 have been performed on the stack I samples. Fig. 4.4 shows the load - displacement curves obtained for the stack I sample with four different barrier types. The curves display the force required for the removal of the Cu film from the substrate which is clearly higher for the two sample with TiWN barriers. Subsequent EDX and optical examination of the peeled surfaces showed that for all investigated samples the interface with the smallest adhesion was between the SiO_2 and the diffusion barrier. Though in practice nitride compounds of refractory metals have shown improved adhesion properties, the related mechanisms are not clear yet. Nitrides in diffusion barriers are commonly used to block possible grain boundaries in the barrier, inhibiting the Cu in using these as diffusion paths [14].

4.4 Fatigue response of copper films on substrate

4.4.1 Influence of the diffusion Barrier

The following experiments were conducted on Cu films of type A - stack I. Fig. 4.5 shows the development of the damage on the surface of copper film on silicon substrates for several samples with TiW and TiWN diffusion barriers subject to a constant loading amplitude ($\frac{\Delta\varepsilon}{2} = 6 \cdot 10^{-4}$). The deformation density as determined from the optical microscope images is plotted versus the number of loading cycles using the intermittent testing procedure described before. All curves show a

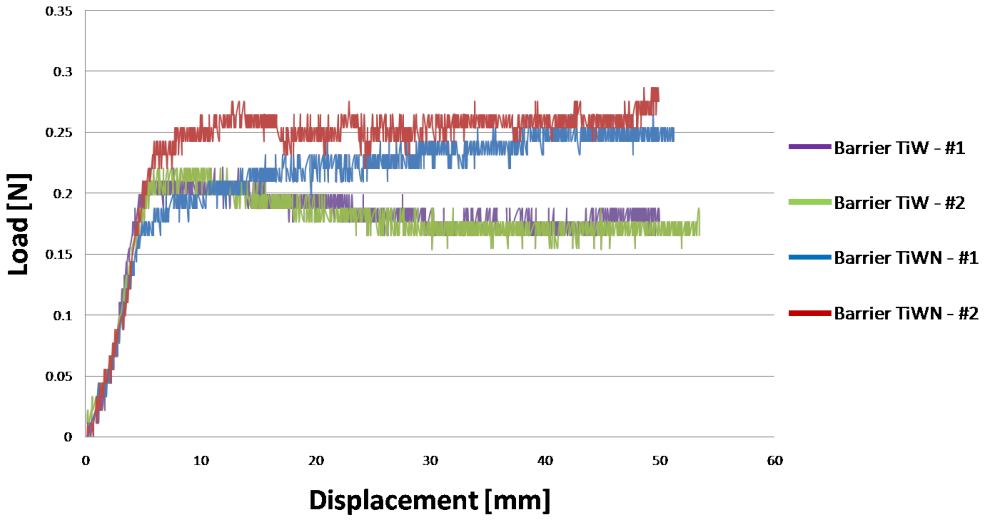

Figure 4.4: The load needed to peel off the film/barrier stack from the substrates indicates a difference in adhesion of the different diffusion barriers to the substrate.

strong increase of the deformation density up to about $2 \cdot 10^8$ cycles during which new deformed areas appear and the existing deformed areas grow in size. Above this region the existing deformed areas grow in size but no new deformed areas appear on the surface. After approximately $2 \cdot 10^8$ loading cycles the slope of the curves slowly decreases indicating a gradual saturation of plastic deformation at about $2 \cdot 10^9$ cycles. Although there is a variance due to the inherently statistical nature of the mechanism of cyclic plastic deformation, one can also see that the curves obtained from samples with a TiWN barrier show a higher density of deformations by trend.

The adhesion can directly or indirectly influence the plastic deformation of the Cu films. During ultrasonic fatigue testing strain is induced in the silicon wafer which is transferred to the adhering Cu film. It is assumed that if the thin Cu film is completely adhered (coupled) to the much thicker silicon substrate the strain induced in the substrate is fully transferred to the Cu film. However this behaviour can be influenced by the adhesive forces at the barrier interfaces. The plot shown in Fig. 4.5 indicates that the weaker adhesion of TiW to the substrate may have resulted in the lower degree of plastic deformation on the surface of the samples. This re-

sult is in conformity with those obtained from the peel tests as shown in Fig. 4.4.

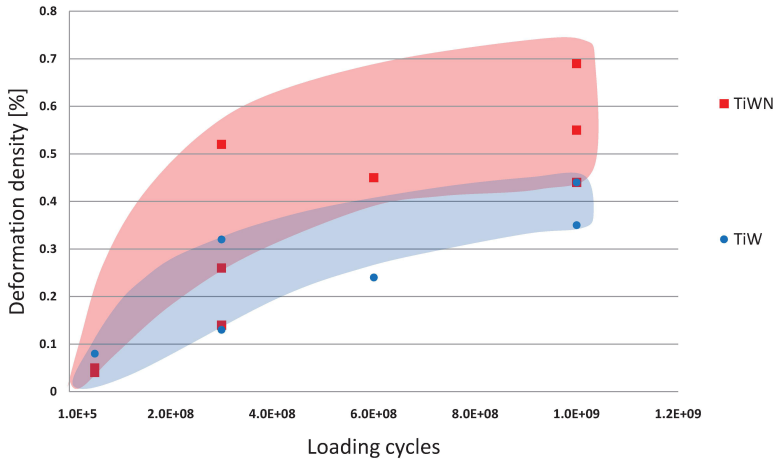

Figure 4.5: The density of deformed grains is influenced by the adhesion of the diffusion barrier to the substrate ($\frac{\Delta\varepsilon}{2} = 6 \cdot 10^{-4}$)

Furthermore a different adhesion influences the intrinsic stress in the Cu films. These intrinsic stresses could shift the threshold needed to achieve plastic deformation in the Cu layers. Thus in case of the fatigue experiments shown in Fig. 4.5, if the externally induced strain in the Cu film is kept constant, higher intrinsic stresses result in a higher degree of plastic deformation in the film. At higher temperatures the amount of intrinsic stresses can be reduced or minimized. Thus further investigations, for example performing fatigue experiments at higher temperatures on these samples, could increase the understanding of the influence of the presence of internal stresses due to the adhesion of the barrier on the deformation mechanisms in Cu films subjected to fatigue loads.

4.4.2 Influence of the microstructure of the Cu films

In order to study the influence of grain size and texture on the fatigue response of Cu films a second set of samples (stack II) was prepared by means of different deposition methods using the same stack layout. For all the samples with the

stack II the copper strip remaining in the middle of the specimen was reduced to 5 mm in order to reduce the residual stress and thereby the transversal oscillation amplitude of the specimen as described in section 3.2.5.

4.4.3 Cu films of type A

The microstructure and layer design of the Cu films of type A - stack II resemble closely the type A - stack I. As shown in Fig. 4.5 fatigue testing at a constant strain amplitude of $6 \cdot 10^4$ resulted in a certain degree of plastic deformation of these Cu films (maximum 0.7 %). In this new series of experiments an improved testing set-up was used in which the additional strain components resulting from the transversal vibration mode of the ultrasonic system were minimized. Fatigue tests conducted at copper films of type A - stack II subjected to an external strain amplitude of $6 \cdot 10^4$ resulted in a very small amount of deformation on the film surface. The deformation density determined for the films of 20 µm thickness was below 0.1 % which was assumed as negligible, and almost no deformed grains were found with samples of 5 µm film thickness. Comparing these results with Cu films of type A - stack I shows the influence of additional transversal strain components on the deformation behaviour of the samples. Because of the inherent statistical nature of fatigue experiments no further quantitative evaluation could be performed.

4.4.4 Cu films of type B

Fig. 4.6 shows the deformation density plotted versus the loading cycles for type B copper specimens with a thickness of 5 µm and 20 µm. It should be noted that the type B samples were subjected only to pure longitudinal vibrations. A significant number of grains showed the typical slip band deformations. Most of the deformed areas appear already very early resulting in a strong increase in deformation density up to about $2 \cdot 10^7$ cycles. By further fatigue loading of the samples the existing deformed areas grow in size leading to a slower slope of the deformation density curve. After about $2 \cdot 10^9$ cycles the deformation density does not increase any

further. The plotted curves also show an approximately 5 times higher deformation density for the 20 µm film compared to the 5 µm film.

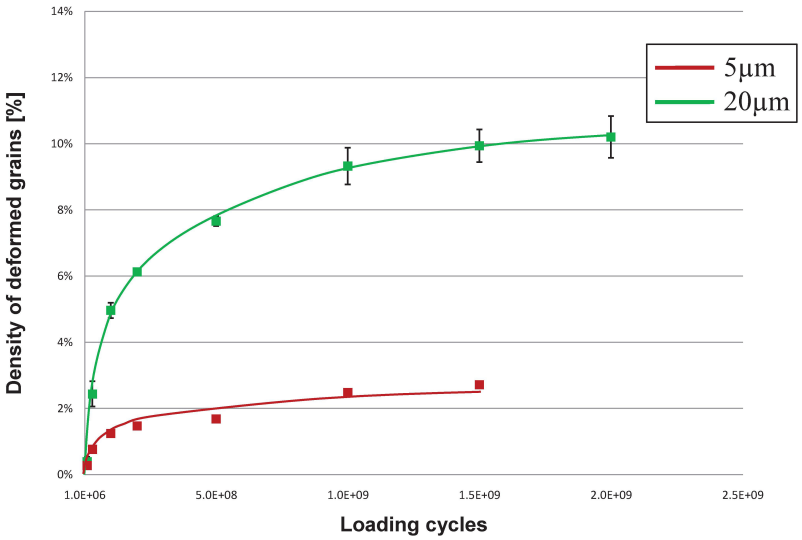

Figure 4.6: Deformation density plotted versus the loading cycles for type B samples

Generally during the thermal cycling of Al thin films a strong change of texture and rotation of grains is observed [27]. Regarding the Cu films this effect is also expected and might even be emphasized by the anisotropy of Cu [28]. In order to compare deformation mechanisms occurring during the mechanical fatigue with thermal cycling, EBSD measurements were performed on defined areas of Cu films before and after fatigue testing. An example of these investigations is given in Fig. 4.7 in which the EBSD images (Euler maps) of the same site of the Cu surface before and after fatigue testing show, that the grain orientation does not change. The white areas are related to the plastically deformed areas which could not be evaluated by the software, due to high surface roughness.

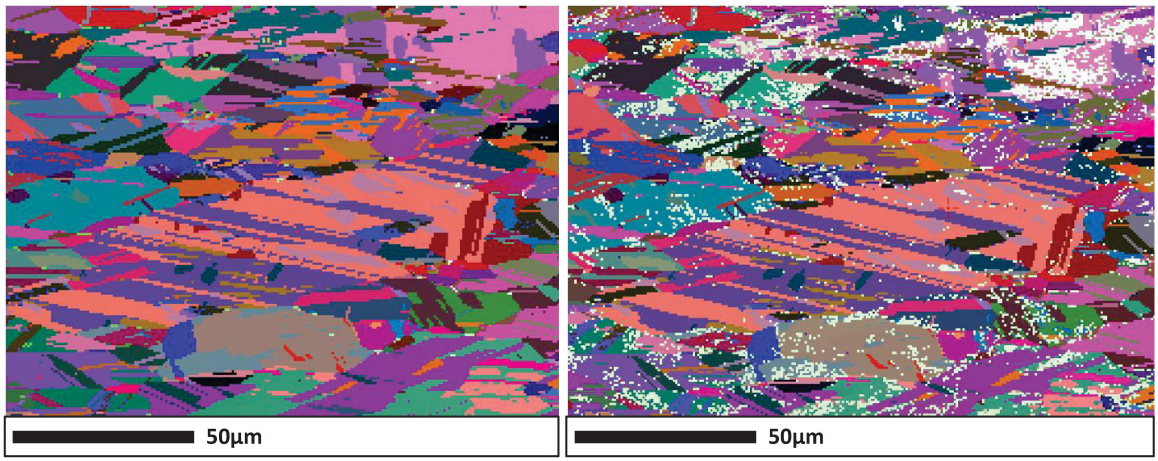

Figure 4.7: Grain orientation map (Euler angles) of the same site before and after fatigue shows no change in grain orientation. White dots in the image of the fatigued sample represent deformed areas

4.4.5 Cu films of Type C

In Figure 4.8 the deformation density of the sputtered type C copper film samples is plotted versus the loading cycles. The increase in deformation density shows a similar behaviour to the type B samples as shown above. The deformation density increases by a factor of 2 to 3 for the thicker films, in this case 10 µm, compared to the thinner films with a thickness of 5 µm.

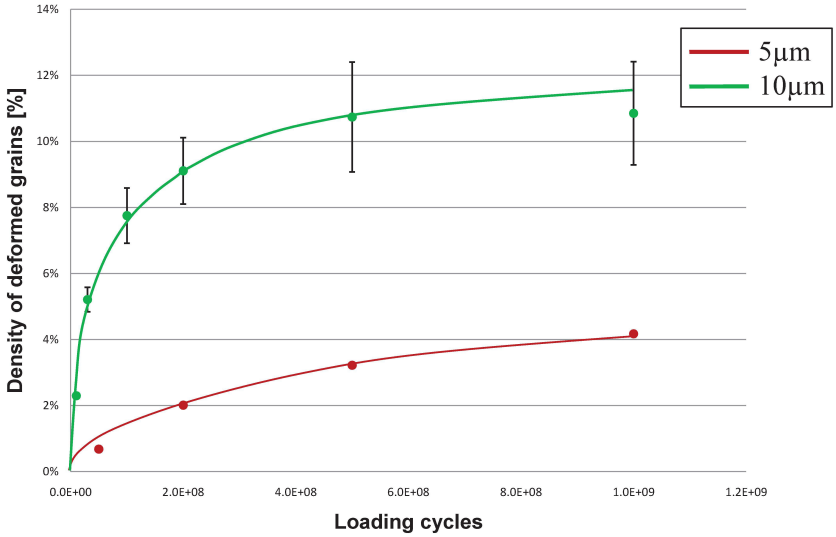

Figure 4.8: Deformation density plotted versus the loading cycles for samples with type C Cu films

4.4.6 Microstructural and dimensional factors influencing the fatigue response of thin films

Figure 4.9 shows the thickness dependency of the ratio of the deformed surface area to the to total area. With all sample types an increase in deformed grains was found with an increased film thickness. However samples of type C films show a clearly higher deformation density.

One can assume that in these films the plastic deformation behaviour is mainly dependent on the thickness, grain size and their ratio, composition and the texture. Films of type B were deposited by electroplating, which yielded a random distribution of grain orientation while the type C samples that were deposited by the sputtering technique showed a strong $\langle 111 \rangle$ preferential orientation.

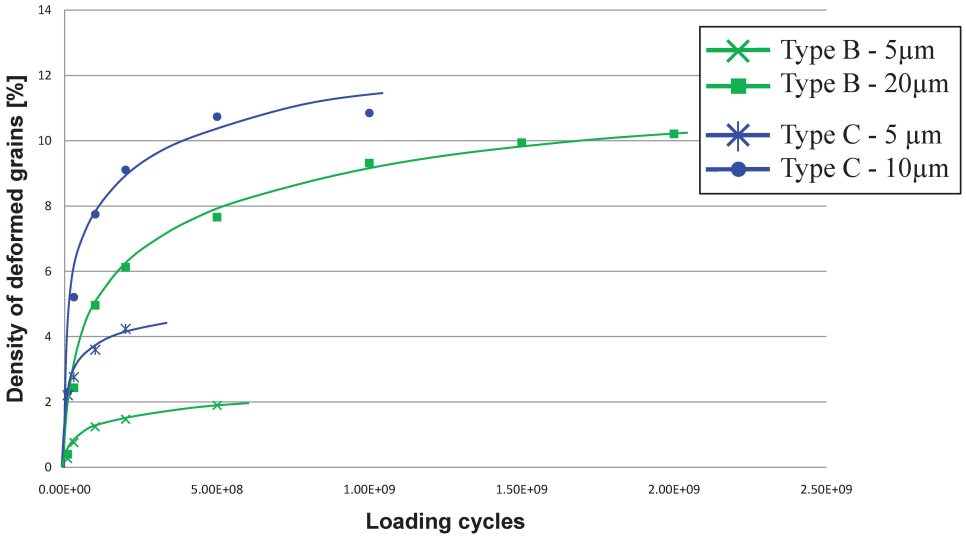

Figure 4.9: Comparison of the deformation density of type B and type C copper indicates a strong orientation dependency of the deformation response.

Influence of grain size

The higher deformation rate observed in coarse grained films is not surprising. It is well know that there is a dependency between the grain and size and tensile response of materials which is described by the Hall-Petch relation. The related mechanisms have been described in chapter 2.6.3 which are also valid for thin films.

Influence of thickness

There are several phenomena proposed to be responsible for this size /constraint effect in fatigue experiments. Nix proposed a model of dislocation channelling, due to the thickness constraint as also described in chapter 2.6.3. Another possible explanation for the fatigue size effect may be connected to the availability and activation of dislocation sources and sinks, which probably depends strongly on film thickness and grain size [36].

Influence of thickness to grain size ratio

Several studies including Miyazaki and Fujita [37] showed that not only the obvious size parameters of the film, namely thickness (d) and grain size (D) themselves, but the ratio of film thickness to grain size ($\zeta = \frac{d}{D}$) strongly influences the mechanical behaviour. They showed that, for thin Cu foils in the thickness range of 45 µm - 1.84 mm, if the ratio (ζ) is below a critical value, which is again dependent on the grain size, the flow stress decreases significantly. For copper foils the critical ratio is higher with smaller grains and is in the order of 5-12. The influence of the film thickness to grain size ratio was explained by the smaller constraints in deformation of the grains near the free surface compared to the grains in the interior of the film.
In a study on cyclic stress-strain response of Cu foils in the thickness range of 50 µm to 250 µm with similar ratio of thickness to grain size ($\zeta \sim 2$) it was found that the cyclic plastic strain is increased with foil thickness. These films were composed of an average of two grains per cross section for all thicknesses, resulting in a smaller near surface volume of the grains in relationship to the whole grain volume for thicker foils. TEM investigations of these samples showed a more homogeneous dislocation distribution inside the grains while heterogeneous dislocation cells were found near the free surface. Results from this study also indicated that an increase of the $\zeta = \frac{d}{D}$ ratio leads to a decrease of the Basquin exponent as grain boundaries again hinder the dislocation movement. (see section 2.6.3) [40].

In our samples the thickness to grain size ratio for both films of type B with thicknesses of 5 µm and of 20 µm was about 1 and lower than that of the type A samples. They showed a ratio of 2 for the sample with 5 µm thickness and 6 for those with 20 µm thickness.

For thin metal films that are confined by a substrate, fatigue mechanisms are different to that of bulk material or free standing foils and wires. The reason for that is the constraining effect of the substrate, which can inhibit dislocation motion as previously shown in section 2.6.3.

In a model described by Zhang et al. [9] three different mechanisms are proposed

to be responsible for the constraint effect. The free surface of the thinner films which is composed of a higher portion of grains may play an important role for dislocation accumulation. In this case the dislocations can escape at the free surface without forming extrusion type deformations in these grains. This is an effect that has also already been proposed in fatigue experiments on thin Cu wires [35]. In the study by Zhang et al. also a minimum length scale for dislocation self-organization was calculated. By taking the values for PSB spacing in copper and estimating the minimum size for dislocation cells and dislocation walls, a critical grain size of 1 μm necessary to form typical dislocation patterns was proposed. A third effect is the constraint on dislocation nucleation and motion due to the small thickness in the film already described in section 2.6.3.

Influence of the orientation

In the present study it was found that the grain orientation plays an important role on the surface damage response of thin Cu films. Fig. 4.9 shows the comparison of deformation density of the mostly $\langle 111 \rangle$ orientated, sputtered type C copper to the randomly orientated type B copper. One can see that the deformation density in the 5 μm films with comparable grain size is twice as high for the type C copper. The deformation density in the type C copper of 10 μm is equally high, or even exceeds that of the twice as thick type B copper film with a thickness of 20 μm.

As in general also with type C copper only a small fraction of all the surface grains show deformation, it is clear that not only the out of plane orientation but also the in plane orientation is highly important. It is well known that the direction of a slip plane to the loading direction plays a major role. Fig. 4.10 a and b show EBSD and SEM images of a type A - stack I Cu film in which the slip direction is indicated, which correspond to the first active slip systems in fcc crystals. The deformed area corresponds here to two grains with $\langle 111 \rangle$ and approximately $\langle 101 \rangle$ out of plane orientation.

This is consistent with findings of other investigators [41, 42, 43]. A study on the thermo-mechanical behaviour of unpassivated Cu thin films on Si substrates

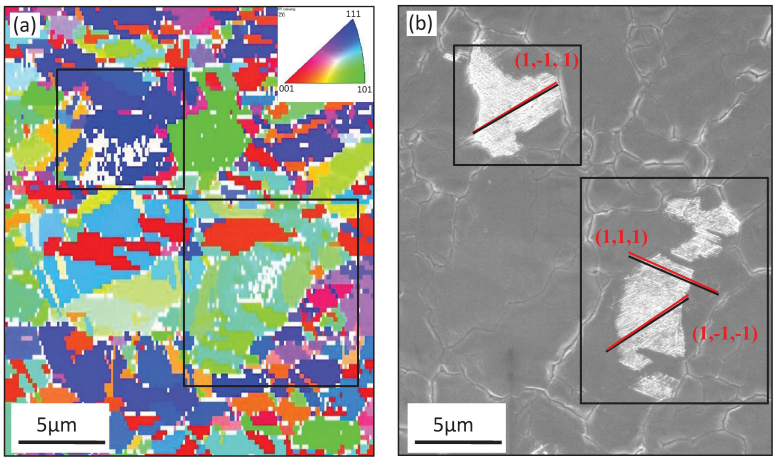

Figure 4.10: (a) IPF map of a Cu surface of a fatigued samples showing two distinct partly deformed grains, the white areas are related to grain boundaries and deformed areas; (b) SEM image of the same site, the black lines indicate the direction of the extrusion lamellas, the red lines represent projections of corresponding slip planes onto the surface.

showed a significantly higher dislocation density in $\langle 100 \rangle$ oriented grains compared to the $\langle 111 \rangle$ grains at room temperature after thermal cycling [43]. They explain that the $\langle 100 \rangle$ oriented grain dislocations hinder the movement of each other, leading to a strengthening of these grains.

The influence of the orientation on the deformation behaviour on Cu films of our study is coherent with the results of a thermal fatigue study by Aicheler et al. [42] in which they report a high stress in $\langle 111 \rangle$-grains compared to $\langle 100 \rangle$ grains as explained by a theoretical model. They state that the $\langle 111 \rangle$ grains experience a higher stress at the same load compared to the $\langle 100 \rangle$ grains due to the isotropy of the coefficient of the thermal expansion, but an anisotropic Young's modulus.

Another study [41] investigated the influence of the texture of thin Cu films for different types of fatigue loading. They compared the damage response of Cu samples thermo-mechanically fatigued by pulsed laser heating and radio frequency induced heating to samples fatigued by an ultrasonic fatigue systems similar to the one used in our study. Their findings indicate again a higher deformation density of the $\langle 111 \rangle$ grains compared to grains of different orientation. This dependency on the grain orientation is less pronounced for the samples subject to uniaxial load,

which is the case for the US fatigued samples, as the in-plane orientation strongly influences the deformation response as well.

4.4.7 Influence of the chemical composition of the electrolyte and the deposition method

The difference in the deformation density of type A and type B copper, especially the 5 µm samples with a comparable grain size and similar orientation makes it apparent that besides length scale effects other factors during the deposition of the copper layers play a significant role for the fatigue lifetime. Both type A and type B copper were deposited by electrochemical-deposition using two electrolytes with different chemical composition. This leads to inclusions of several foreign atoms in the copper layers. Measurements of the percentage of foreign atoms as Cl and S showed a smaller number in type B compared to type A copper [44]. This larger number of inclusions/impurities/voids in the type A copper could also affect the slip movement as foreign atoms can inhibit the dislocation motion.

4.4.8 Fatigue damage

In this section an overview of the microstructural investigations and the damage evolution and fatigue damage features of the different Cu films is given.

Figure 4.11 shows an overview of the surface of the three different types of copper films used in this study with different thickness at the initial state. Fig 4.11 a and b show type A copper of 5 µm and 20 µm thickness respectively. The type B copper shown in Fig. 4.11 c, d shows comparable surface roughness to the type A copper but with much larger grains for the 20 µm thick film. The sputtered copper, type C (Fig. 4.11 e, d) shows deeper grooves at the grain boundaries.

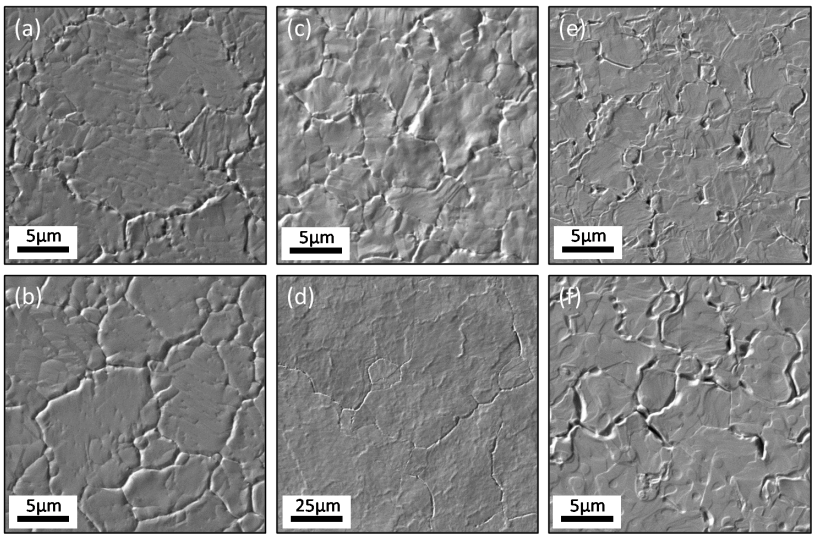

Figure 4.11: SEM images of type A (a) 5 µm, (b) 20 µm, type B (c) 5 µm (d) 20 µm and type C (e) 5 µm, (f) 10 µm before cycling.

Detailed SEM investigations of the fatigued samples showed that after about $1 \cdot 10^7$ cycles fine extrusions appear on the surface of all types of tested thin films as shown in Fig. 4.12.

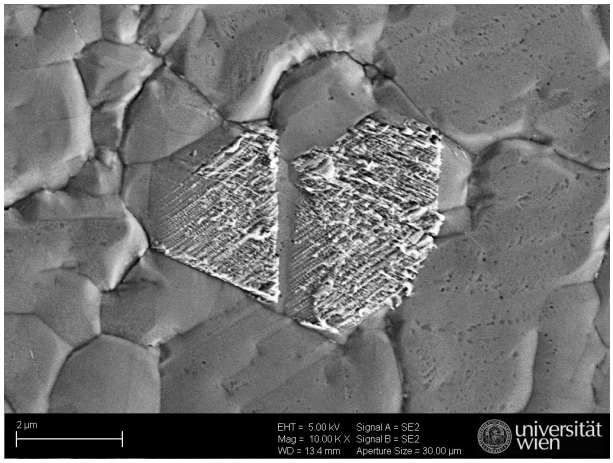

Figure 4.12: SEM image of extrusions on a type A - stack I fatigued film ($\frac{\Delta\varepsilon}{2} = 6 \cdot 10^{-4}$, $N = 1.3 \cdot 10^9$ cycles).

These extrusions are always formed within single grains, and also seem to be

stopped by twin boundaries. EBSD measurements and electron channelling contrast examination of the surface showed that the extrusions are mostly generated along the $\{111\}$ slip planes indicating that at the given strain amplitude slip was activated only in the grains with the highest Schmid factor. As the number of cycles is increased more extrusions appear while the existing extrusions grow in size until about $2 \cdot 10^8$ cycles. After that no new deformations appear on the surface, while the existing deformed areas still grow in size up to approximately $2 \cdot 10^9$ cycles after which the maximum is reached and the deformation density goes into saturation.

The SEM images in Fig 4.12 show the slip band formation on the type A - stack I copper after fatigue testing ($\frac{\Delta\varepsilon}{2} = 6 \cdot 10^{-4}$, N = $1.5 \cdot 10^9$). It can be seen that the extrusion lamellas often appear in two different directions mostly oriented with an angle of 45° to the loading direction. It was also often observed that two slip systems are activated crossing each other at a certain angle. It can also be seen that there is a very distinct edge between the extrusion at grain and twin boundaries. The undamaged areas show the original surface of the film.

The fatigued Cu surface of a type B 20 µm thick Cu film and its damage structure is shown in Fig. 4.13. In addition to the much higher deformation density also the damage morphology is slightly different to that of the type A copper. The extrusions are much finer compared to the type A Cu, showing a faceted nodular structure.

The SEM image in Fig. 4.14 shows the surface damage of the type C copper films. Thin slip band deformations often cover whole grains as well as some small initial cracks appear at grain or twin boundaries.

Focused Ion Beam (FIB) techniques were used to prepare cross sections of the fatigued films in order to investigate the shape and the dimensions of the extrusions and the interaction of the extrusions with the interface to the substrate. The investigations were focused on sites perpendicular to the surface traces of the extrusion. As shown in Fig. 4.15 the surface markings are still visible and one can estimate

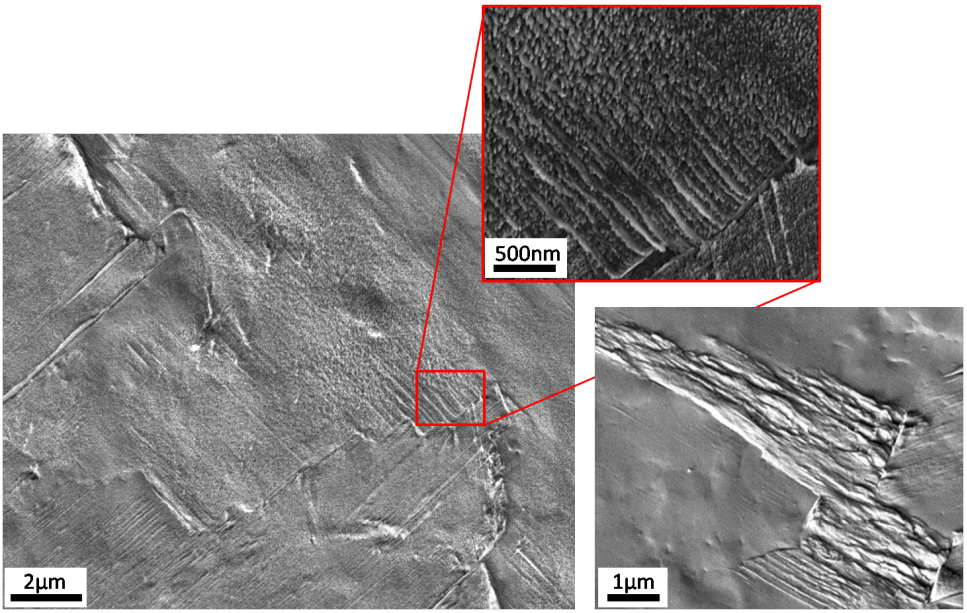

Figure 4.13: SEM images of the surface deformations of a type B sample of a thickness of 20 µm ($\frac{\Delta\varepsilon}{2} = 6 \cdot 10^{-4}$, $N = 1.5 \cdot 10^9$ cycles).

the extrusion height to be in the range of 0.1 µm. One can also see traces of the extrusions forming small cracks inside of this grain beneath the extrusions.

Beneath the extrusion small voids were also observed at the grain boundaries shown in Fig. 4.16. These voids could be interpreted as the agglomeration of vacancies resulting from the transport of material to the free surface. Although some larger voids can be seen randomly scattered in the FIB images as well, the voids at the boundaries of the deformed grains show a higher density. Further investigation will be needed to confirm this hypothesis.

Examination of the FIB cross sections of several samples (Fig. 4.17 and 4.18) showed that the extrusions are terminated within the grains (e.g. 1 µm length for the 5 µm samples and approximately 4 µm for the 20 µm samples). They did not reach the interfaces to the silicon and no void formation at Cu/barrier interface was observed.

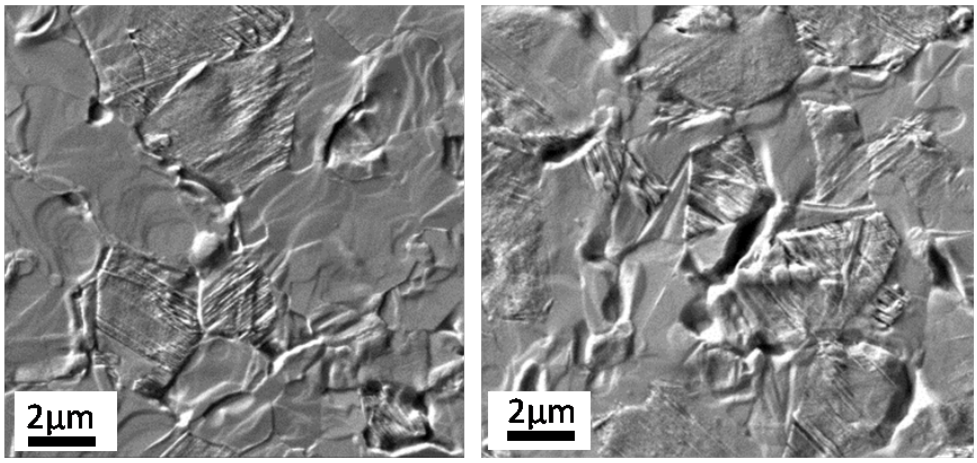

Figure 4.14: SEM images of the surface deformations of type C samples (a) 5 µm (b) 10 µm. (both $\frac{\Delta\varepsilon}{2} = 6 \cdot 10^{-4}$, $N = 1.5 \cdot 10^9$ cycles).

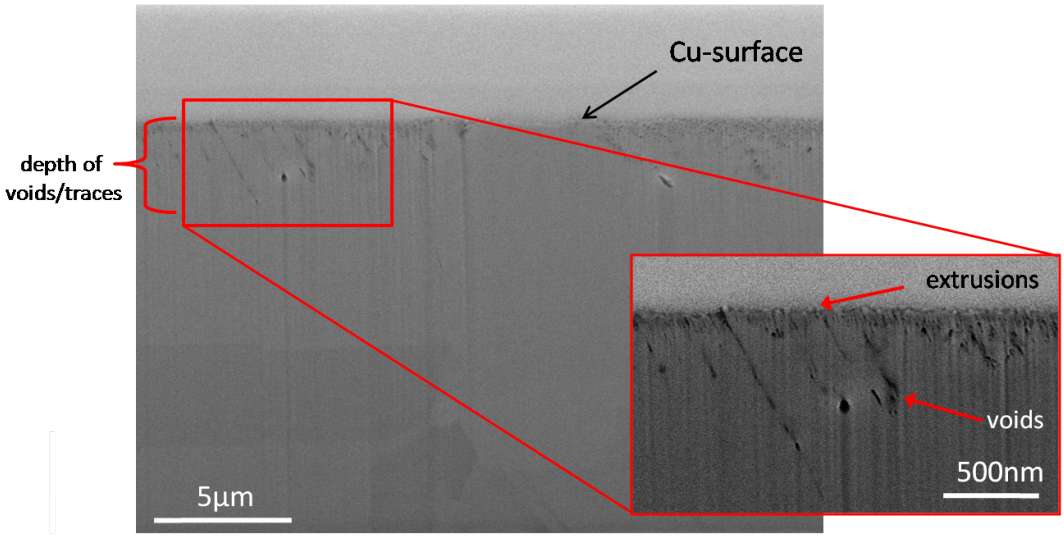

Figure 4.17: FIB image at 45° tilt of a type B 20 µm fatigued sample ($\frac{\Delta\varepsilon}{2} = 6 \cdot 10^{-4}$, $N = 1.5 \cdot 10^9$).

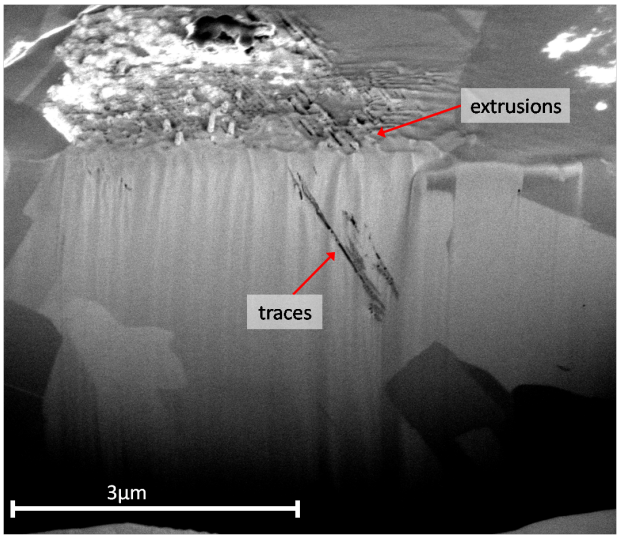

Figure 4.15: FIB image at 52° tilt of a type A -stack I fatigued sample ($\frac{\Delta\varepsilon}{2} = 6 \cdot 10^{-4}$, $N = 1.3 \cdot 10^9$). The deformations on the surface extend into the interior of the surface grains.

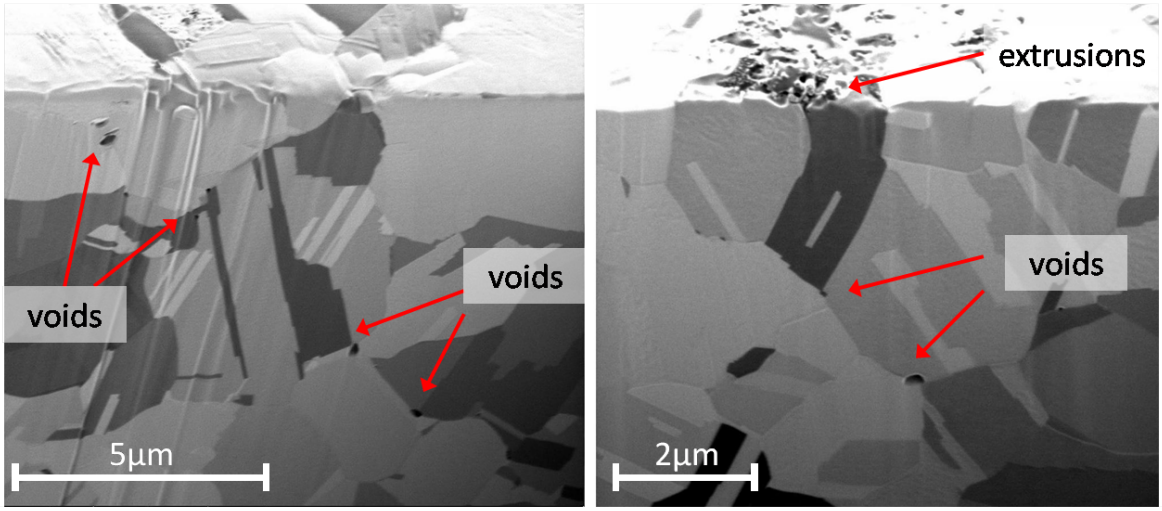

Figure 4.16: FIB image at 45° tilt of a type A - stack I fatigued sample ($\frac{\Delta\varepsilon}{2} = 6 \cdot 10^{-4}$, $N = 1.3 \cdot 10^9$).

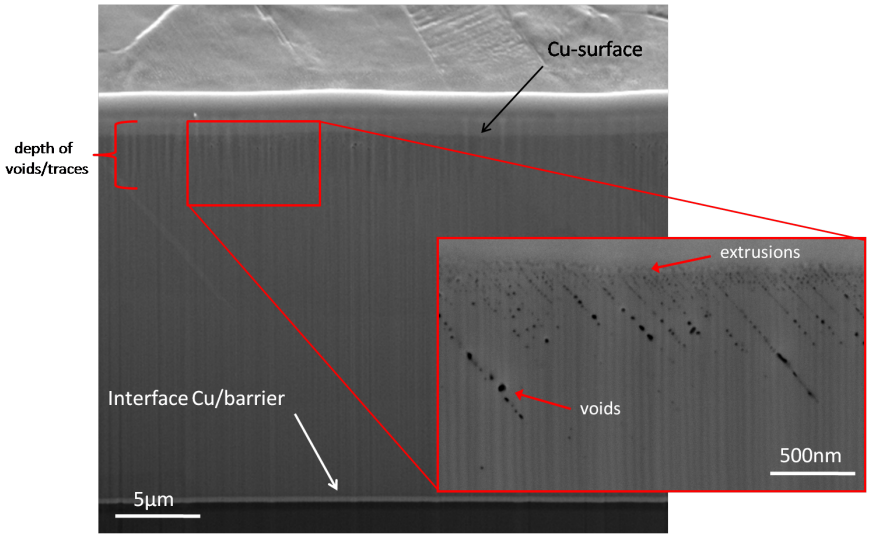

Figure 4.18: FIB image at 45° tilt of a type C 5 µm fatigued sample ($\frac{\Delta\varepsilon}{2} = 6 \cdot 10^{-4}$, $N = 1.5 \cdot 10^{9}$).

Similar features were observed in bulk copper samples which were subjected to cyclic loading in the very high cycle region at stress levels far below the fatigue limit. In a study by Phung et al. [45] different types of surface slip markings were found predominantly at different stress amplitudes. For higher stress amplitudes (> 65 MPa) long, straight persistent slip markings in small clusters that cross the grain boundaries appeared, while at medium amplitude (45-65 MPa) long isolated slip markings were found. The third type of slip markings were observed at lower stress amplitudes (<45 MPa) that very much resemble our surface features. Clusters of very fine slip markings were built within the grains, within which two slip directions often appeared with one direction being more pronounced than the others. These slip markings, much as ours show only a small roughness in the range of several nanometres. SEM images of these slip markings with a comparison to the surface features of our samples are given in Fig. 4.19.

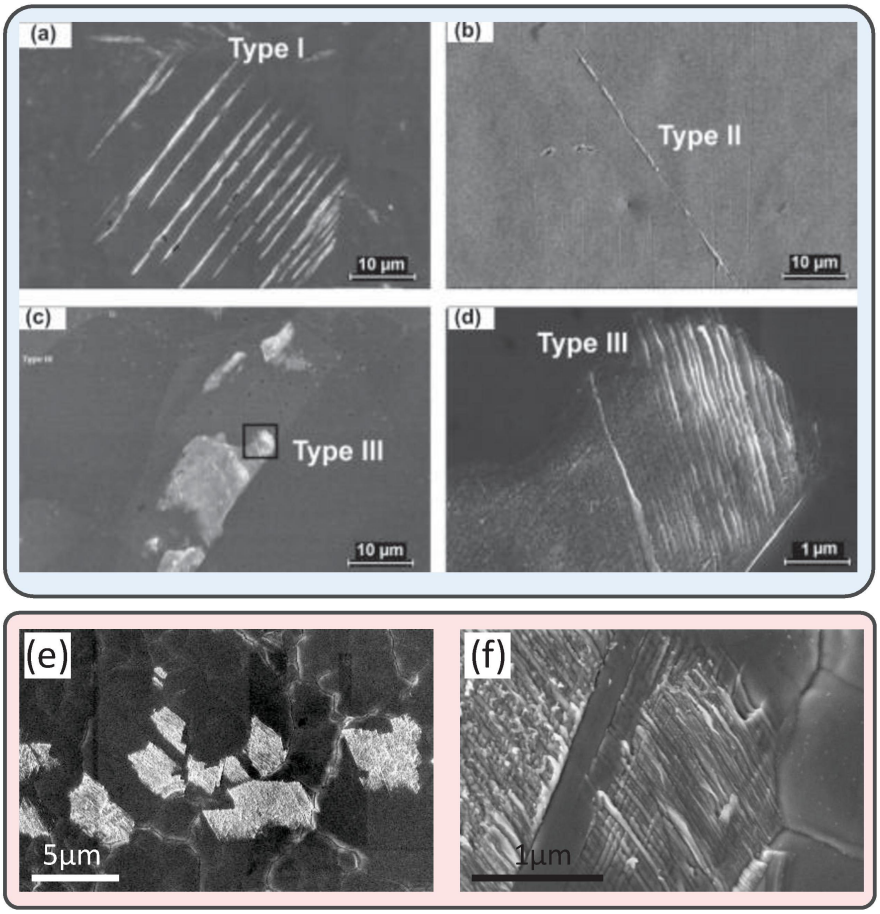

Figure 4.19: Comparison of the damage morphology of our samples (e,f) to a study on HCF behaviour of Cu samples of bulk copper by Phung et al. with three types of slip markings generated by fatigue loading at different strain amplitudes (a-d) [45].

Investigations by Zhang et al. [10] on the fatigue response of Cu films with a thickness range from 200 nm to 3 µm on a polyimide substrate with various microstructure and by Burger et al. [31] on Al and Cu films of 1 µm thickness on a Si substrate showed that extrusion formation at the surface led to void formation inside the grains and at the film/substrate interface (Fig. 4.20). The lack of such voids at our film-substrate interfaces could be explained due to a lower plastic strain by a factor of 10 in our experiments at the very high cycle region.

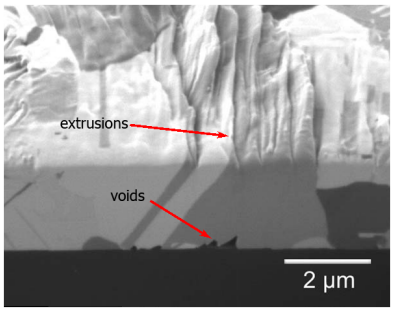

Figure 4.20: FIB image of a 3 µm thick Cu film on a polyimide substrate after fatigue tests performed by Zhang et al. [10] showing extrusions on the surface and voids at the film-substrate interface ($\frac{\Delta\varepsilon}{2} = 1\,\%$)

Both observations and comparison of the damage response on the surface and inside the films lead to the conclusion, that the strain amplitude of $6 \cdot 10^{-4}$ ($\sim$72 MPa) is rather low for our thin Cu films on the substrate and that the rigid substrate enhances the fatigue resistance of the multilayer thin film samples as will be discussed in the next section .

4.5 Free standing Copper bars

4.5.1 Fatigue lifetime

Using the ultrasonic resonance systems described in chapter 3.2.1 the free standing Cu bars were subjected to fatigue loading until failure. The S-N curves obtained for Cu films of type A and B are shown in Fig. 4.21 in which the strain amplitude against the loading cycles is plotted. Arrows marking some of the measured points indicate specimens without rupture (run-outs). The strain amplitude in the lifetime curve of the fine grained type A ranges from about $2.8 \cdot 10^{-4}$ at the lowest number of cycles ($N = 5 \cdot 10^5$) to $2.5 \cdot 10^{-4}$ at the maximum number of cycles ($N = 2 \cdot 10^9$). As expected in the HCF/UHCF regime the slope of this curve is rather flat. Though the lifetime measurements for type B experiments are limited mainly to the region up to 10^6 due to the lack of samples, the results clearly show an improved fatigue

response of fine grained Cu samples (type A) in comparison with their coarse grained counterparts (type B).

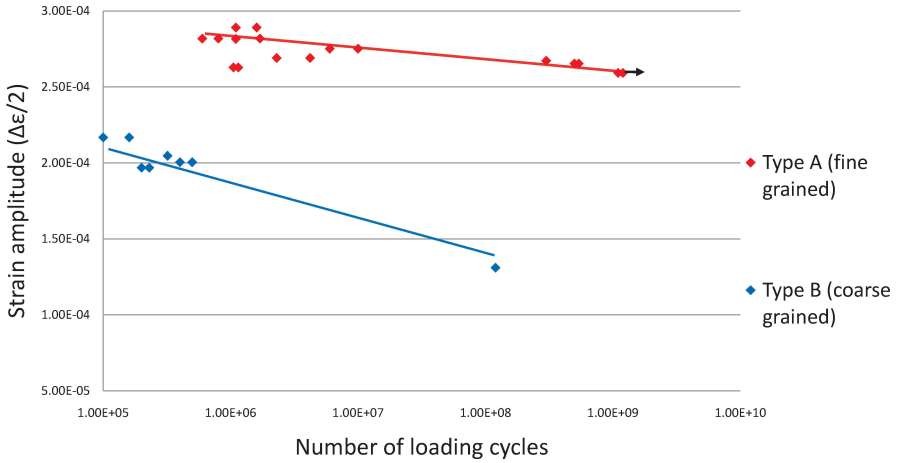

Figure 4.21: S-N curve of 20x20 µm free standing type A and type B copper bars

4.5.2 Fatigue damage

SEM investigations were conducted on fatigued samples in order to investigate the damage mechanisms responsible for failure of the free standing Cu bars. The surface damage of a failed type A free standing copper bar after $1.8 \cdot 10^7$ cycles with $\frac{\Delta\varepsilon}{2} = 2.66 \cdot 10^{-4}$ is shown in Fig. 4.22 The SEM image displays deep extrusion clusters in almost all grains within the whole gauge length. Similarly to the Cu on the substrate these extrusions lamellas are mostly oriented in an angle of 45° with respect to the fatigue direction. The SEM images in Fig 4.23 show the surface of a type B free standing Cu bar before and after fatigue. The sample failed after $1.2 \cdot 10^8$ cycles at a constant strain amplitude of $\frac{\Delta\varepsilon}{2} = 1.4 \cdot 10^{-4}$. The extrusion lamellas are much finer compared to the type A samples stretching across the whole width due to the large grain size.

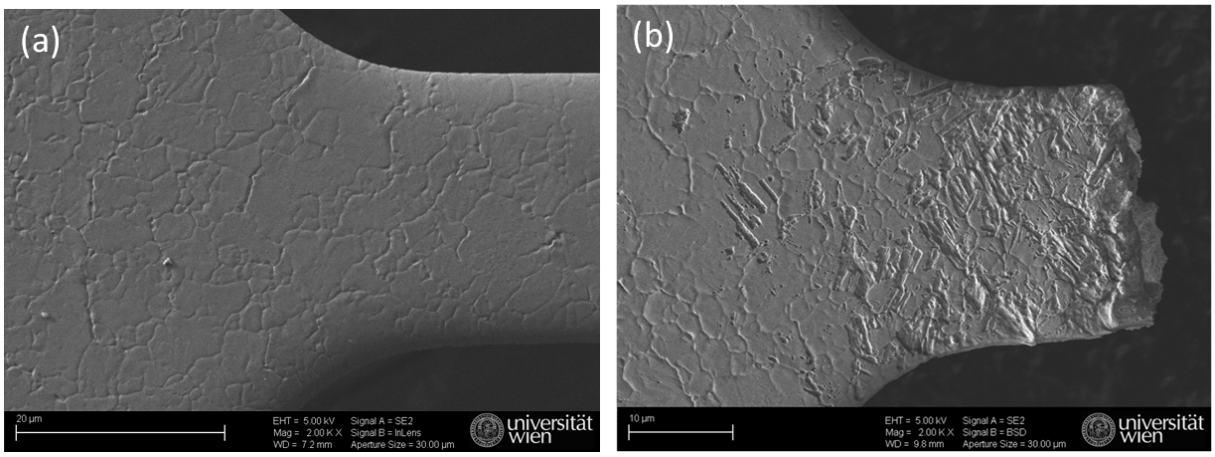

Figure 4.22: SEM micrographs of the type A free standing copper bars (20 µm x20 µm (a) before (b) after fatigue ($\varepsilon = 2.66 \cdot 10^{-4}, N = 1 \cdot 10^{7}$) deep, broad intrusions on almost all grains

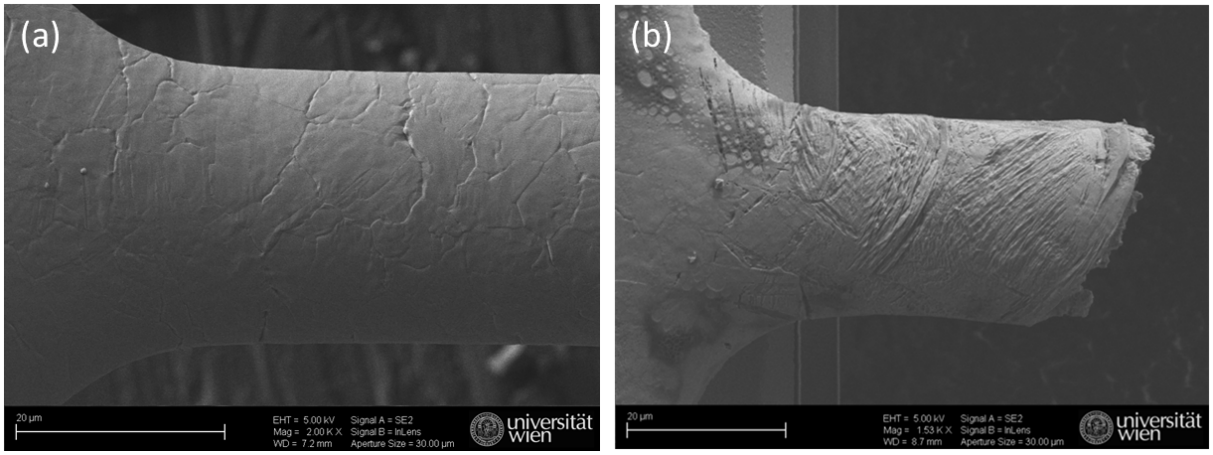

Figure 4.23: SEM micrographs of the type A free standing copper bars (20 µm x20 µm (a) before (b) after fatigue ($\varepsilon = 1.4 \cdot 10^{-4}, N = 1.2 \cdot 10^{8}$) narrow intrusions across the copper bar

Fig. 4.24 shows a comparison of the fatigue lifetime with fatigue experiments on small bamboo structured copper wires, similar to the coarse grained type B copper bars [35]. One can see that samples with similar diameters show comparable results.

In the study by Khatibi et al. the results indicated a Hall-Petch like increase of the yield strength with decreasing wire diameter.

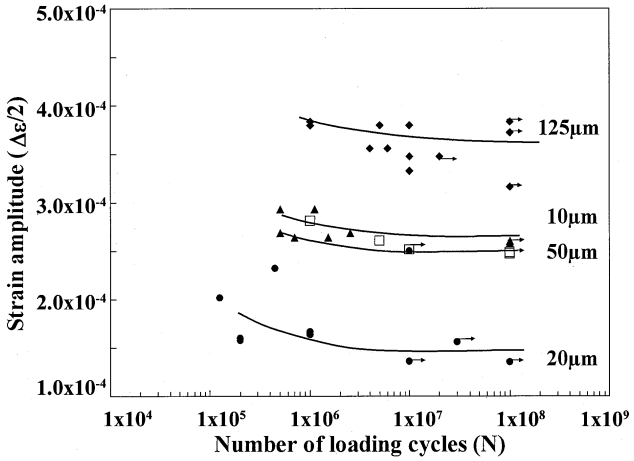

Figure 4.24: Relationship between strain amplitude and the number of cycles to failure for Cu micro wires with different diameter. [35]

Also the deformation with the slip band structure, resemble the deformation of the coarse grained copper bars very well. The slip band structure of the deformation of these Cu wires is shown in Fig. 4.25.

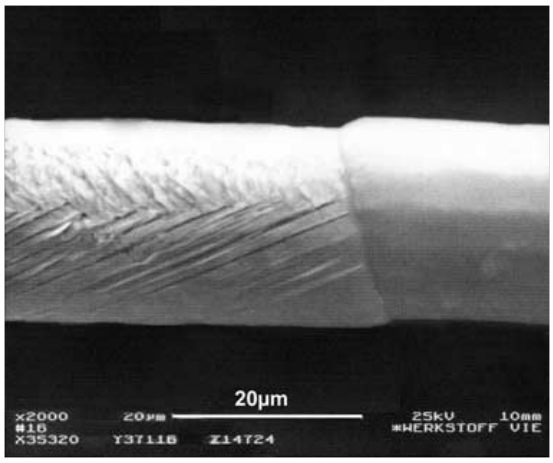

Figure 4.25: Sem micrograph of the intrusions on deformed grains of a microwire of 20 µm diameter ($\varepsilon = 1.4 \cdot 10^{-4}, N = 10^7$). [35]

Comparing the results of our study with tensile tests and low cycle fatigue experiments performed on the same free standing copper bars by A.Wimmer et al. [6], a similar trend for the electro deposited copper is shown. Equal to our results the fine grained (type A) copper shows a higher fatigue limit than the coarse grained (type B) copper (Figure 4.26). Also both S-N curves, especially for the coarse grained material, show the same rather gentle slope.

Differences of the absolute value of the fatigue strength can be explained by the different experimental conditions (Table 4.2). While our experiments were performed under completely reversed cyclic loading ($R = -1$) the cyclic tests in the LCF study were under tensile-tensile ($R \approx 0$) loading which strongly affects fatigue life as already described in section 2.7. Also the much lower frequency of 0.05 Hz compared to our 20kHz and the influence of the environment, as our experiments were performed at air whereas the testing of the LCF study was performed in vacuum contribute to the different absolute values. It is known that the environmental conditions affect the fatigue life of materials. Exposing the material to ambient air decreases the fatigue life significantly compared to fatigue in vacuum. During the cyclic loading slip steps appear on the surface and an oxygen layer forms almost immediately on the freshly exposed metal surface. This formation of an oxide makes reverse slip difficult on the same slip plane upon load reversal. This effect becomes amplified at higher temperatures and with increasing humidity of the ambient air [2].

Additionally, as shown in section 2.7, Fig 2.11, it is assumed that many ductile materials do not show a linear drop over the whole range of loading cycles in fatigue curves, but rather show a multiple step behaviour. That means that linear extrapolations from LCF experiments such as the ones from Wimmer et al. could overestimate the factual strain limit in the HCF range of our fatigue tests.

LCF	HCF
in vacuum	at ambient air
mean stress > 0	mean stress = 0
low frequency (0.1 Hz)	high frequency (20kHz)

Table 4.2: Comparison of the testing conditions

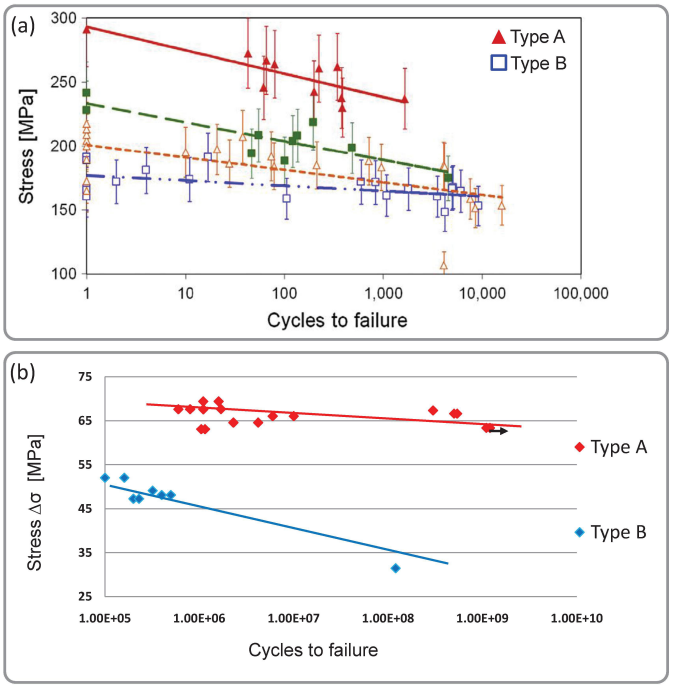

Figure 4.26: Comparison of stress lifetime curves of 20x20 µm free standing copper bars of (a) a LCF study [6] and (b) our UHCF/HCF study. It should be noted that for better compearability the caption of the LCF study has been adapted, and in both cases $\Delta\sigma = 2 \cdot \Delta\sigma_A$ is plotted vs. the loading cycles.

4.6 Comparison of free standing Cu bars to Cu films on substrate

The damage response of free standing copper bars and Cu films of the same microstructure on a rigid structure shows a significant difference. Although the strain amplitude ($\frac{\Delta\varepsilon}{2} = 6 \cdot 10^{-4}$) for the Cu films on substrate fatigue tested in this study was significantly higher compared to the free standing bars ($\frac{\Delta\varepsilon}{2} = 1.5 \cdot 10^{-4}$) the constraint of the substrate inhibits dislocation movement resulting in a much lower deformation density.

Chapter 5

Conclusions

In this section the experimental methods, the main findings and the conclusions of this thesis are presented.

In this study mechanical fatigue behaviour of different types of Cu metallization film stacks (consisting of Si/SiO_2/TiW/Cu) on Si substrates was investigated in the high cycle fatigue regime at room temperature. For this purpose an ultrasonic fatigue set-up working at 36 kHz was used. Qualitative and quantitative evaluation of the surface of Cu films subsequent to fatigue loading was conducted by means of optical- and electron microscopy and the density of deformed surface grains as a function of loading cycles for all types of samples were determined.

In addition to the Cu films on the Si substrate, free standing copper bars of the same microstructure have been fabricated and were subjected to fatigue load using an ultrasonic fatigue system working at 20kHz. This system has already shown its applicability for several fatigue studies for small scaled samples [32, 35]. The same kind of specimen have been used for investigations on tensile behaviour, especially the temperature influence, and LCF experiments [5, 6].

The investigations on the thin film copper samples on silicon substrates lead to the conclusion that various parameters influence the fatigue damage response of the Cu metallization:

- The experimental results show that with increasing the film thickness from 5 μm up to 10 μm and 20 μm, respectively, the deformation density increases

significantly. This influence seems to be independent of a change in grain size and microstructure.

- Besides the film thickness the grain size is another dimensional factor influencing the damage response. A smaller grain size can also inhibit dislocation motion and therefore lead to less damage on the Cu surface.
- It was found that an out of plane orientation in the $\langle 111 \rangle$ direction strongly increases the slip band formation in the Cu films. Thus sputtered films with a dominant $\langle 111 \rangle$ orientation showed a higher degree of cyclic plastic deformation.
- Peel test measurements in combination with the fatigue experiments also indicated that the interfacial adhesion between the diffusion barrier layer and the substrate can also influence the damage response of the film stack. During the fatigue loading interfaces with higher adhesion strength seem to transfer the stress induced in the Si substrate to the Cu film more efficiently leading to a higher surface degradation by trend.

In addition to the fatigue tests on the film stacks, free standing copper bars of the same microstructure were fabricated and fatigued to further investigate the constraining effect of the substrate. It was found that the free standing Cu bars showed a significantly lower fatigue resistance than Cu films on Si substrates. Comparing the degree of surface damage in free standing and constraint samples, plastic deformation occurred in most of the grains of the Cu bars, at much lower loads clearly indicating a strong constraining effect of the rigid Si substrate on deformation of Cu films. The fatigue life experiments on these free standing samples also indicated a lower fatigue limit of the fine grained to that of coarse grained copper which is consistent with results from a study on LCF experiments on the same kind of free standing copper bars [6]. The difference in the absolute value can be explained by the different experimental conditions and a nonlinear behaviour of the S-N curve for ductile materials such as copper resulting in a drop from the LCF to the (U)HCF range. The LCF experiments were performed with a load ratio $R \sim 0$ at very low frequencies in vacuo influencing the lifetime of the copper bars significantly. The surface damage of the LCF samples also showed

significant differences, as the typical extrusion/intrusion structure was not found, but rather surface evolution similar to the damage found after tensile testing.

5.1 Outlook

The results of our study raise further questions that may be answered by additional follow up investigations. During the operational life Cu metallization films are subjected to temperature cycles in the range of minus 40°C to about 250°C . Since the stress-strain and fatigue response of copper is strongly temperature dependent, it would be interesting to conduct the experiments at higher temperatures to get further insight in the thermo-mechanical fatigue behaviour. The type of slip band formation and the degree of surface damage of the Cu films stacks in this study indicated that the applied strain amplitude during the fatigue experiments was rather low. Performance of fatigue tests at higher strain amplitudes could contribute to a better understanding of the mechanical fatigue response of Cu films on the Si substrate.

The present study shows that the ultrasonic resonance fatigue testing system is a very efficient method for mechanical fatigue testing of small scale samples of various geometry and structure.

Chapter 6

Bibliography

[1] M. Aoki et al. *Fabricating 3D Integrated CMOS Devices by Using Wafer Stacking and Via-last TSV Technologies* Proceedings Electron Devices Meeting (IEDM), 2013 IEEE International 29.5.1 - 29.5.4

[2] W.D. Nix *Elastic and plastic properties of thin films on substrates: nanoindentation techniques.* Materials Science and Engineering A, 234?236 (1997), 37?44

[3] R.M. Keller, S. Baker, E. Arzt *Stress-temperature behaviour of unpassivated thin copper films.* Acta Materialia, Volume 47 (1999), 415-426

[4] E.Arzt *Size effects in materials due to microstructural and dimensional constraints: a comparative review*. Acta Mater (1998) 46:5611-5626

[5] M.Smolka, C.Motz, T.Detzl, W.Robl, T.Griesser, A.Wimmer, G.Dehm *Novel temperature dependent tensile test of freestanding copper thin film structures.* Review of Scientific Instruments 83 (2012) 064702.

[6] A.Wimmer, A.Leitner, T.Detz, W.Robl, W.Heinz, R.Pippan, G.Dehm *Damage evolution during cyclic tension-tension loading of micron sized Cu lines* Acta materialia 67 (2014) 297-307

[7] D.Wang, C.Volkert, O.Kraft *Effect of length scale on fatigue life and damage formation in thin Cu films* Materials Science and Engineering 493 (2008) 267-273

[8] O.Kraft, P.Gruber, R.Mönig, D. Weygand *Plasticity in confined dimensions* Annu. Rev. Mater. Res. (2010) 40:293-317

[9] G.P.Zhang, C.A.Volkert, R.Schwaiger, P.Wellner, E.Arzt, O.Kraft. *Length-scale-controlled fatigue mechanisms in thin copper films*. Acta Materialia 54 (2006) 3127-3139.

[10] G.P.Zhang, C.A.Volkert, R.Schwaiger, R.Mönig, O.Kraft. *Fatigue and thermal fatigue damage analysis of thin metal films*. Microelectronics Reliability 47 (2007) 2007-2013.

[11] R.Mönig, R.Keller, C.A.Volkert *Thermal fatigue testing of thin metal films* Review of Scientific Instruments Volume 75 Issue 11 (2004) 4997-5004

[12] Y.B.Park, C.A.Volkert, R. Mönig *Thermal fatigue as a possible failure mechanism in copper interconnects.* Thin Solid Films, 504 (2006) 321-324.

[13] W.Robl, M.Melzl, B. Weidgans, R.Hofmann, M.Stecher *Copper Metallization for Power Devices* ASMC (Advanced Semiconductor Manufacturing Conference Proceedings (2007) 259-262

[14] Semant Rawal *Alternative Nitride diffusion barriers on silicon and germanium for copper metallization*

[15] M.Ohring *The Materials Science of Thin Films* Academic Press, Inc., (1992)

[16] G.G.Stoney *The tension of metallic films deposited by electrolysis* Proceedings of the Royal Society London A 82 (1909) 172-175

[17] P.A. Flinn *Measurement and interpretation of stress in copper films as a function of thermal history* Journal of Materials Research, Volume 6, Issue 7 (1991) 1498-1501

[18] S.Suresh. *Fatigue of Materials* Cambridge University Press (1991)

[19] A.G.Evans. *Adhesion Measurements of Films & Coatings Volume 2* Editor: K.L.Mittal VSP 2001

[20] Z.Chen, K. Zhou, X.Lu, Y.C.Lam *A review on the mechanical methods for evaluating coating adhesion* Acta Mech. 225 (2013) 431-452

[21] D.Hull, D.J.Bacon *Introduction to dislocations*. Oxford: Butterworth-Heinemann 4th Edition, (2001)

[22] W.D.Nix *Mechanical Properties of thin films* Metallurgical transactions A - Physical Metallurgy and materials science 1989, volume 20A 2217-2245

[23] V.Weihnacht, W.Brückner *Dislocation accumulation and strengthening in Cu thin films* Acta Materialia Volume 49, Issue 13 (2001) 2365?2372

[24] C.V. Thompson *The Yield Stress of Polycrystalline Thin Films.* Journal of Materials Research (1993) 237-238.

[25] B. von Blanckenhagen, P.Gumbsch, E.Arzt *Dislocation sources in discrete dislocation simulations of thin film plasticity and the Hall-Petch relation* Modelling Simul. Mater.Sci.Eng, volume 9 (2001) 157-169

[26] Y.Xiang, T.Li, Z.Suo,J.J.Vlassak *High ductility of a metal film adherent on a polymer substrate* Applied Physics Letters 87 (2005) 161910

[27] W.Heinz, R.Pippan, G.Dehm *Investigation of the fatigue behaviour of Al thin films with different microstructure* Materials Science and Engineering A, volume 527, issue 29-30 (2010) 7757?7763

[28] H.M.Ledbetter, E.R.Naimon *Elastic properties of metals and alloys. II. Copper* Journal Phys. Chem. Ref. Data, Volume 3, 1974

[29] L.D.Roth *Ultrasonic fatigue testing* Metals Handbook , volume 8, 9th edition (1985) p.240

[30] Walter D.Pilkey, Deborah F.Pilkey. *Peterson's stress concentration factors*. John Wiley and Sons, 3rd Edition, (2008).

[31] S.Burger, C.Eberl, A.Siegel, A.Ludwig, O.Kraft *A novel high-throughput fatigue testing method for metallic thin films* Sci. Technol. Adv. Mater. Volume 12 (2011) 054202

[32] G.Khatibi, J.Horky, B.Weiss, M.J.Zehetbauer. *High cycle fatigue behaviour of copper deformed by high pressure torsion*. International Journal of Fatigue 32 (2010) 269-278.

[33] H.Mughrabi. *Specific Features and Mechanisms of Fatigue In the Ultrahigh-Cycle Regime*. International Journal of Fatigue 28 (2006) 1501-1508.

[34] A.Weronski, T.Hejwowski *Thermal Fatigue of Metals* Marcel Dekker, Inc. New York (1991)

[35] G.Khatibi, A.Betzwar-Kotas, V.Gröger, B.Weiss *A study of the mechanical fatigue properties of metallic microwires*. Fatigue & Fracture of Engineering Materials & Structures 28 (2005) 723-733

[36] B. von Blanckenhagen, P.Gumbsch, E.Arzt *Dislocation sources and the flow stress of polycrystalline thin metal films.* Phil. Mag. Lett. Volume 83 1-8, 2003.

[37] S. Miyazaki, H. Fujita *Effects of grain-size and specimen thickness on mechanical-properties of polycrystalline copper and copper-aluminium alloy* Transactions of the Japan Institute of Metals (1979) 439- 444.

[38] Rasband, W.S., ImageJ, U. S. National Institutes of Health, Bethesda, Maryland, USA, http://imagej.nih.gov/ij/, 1997-2012.

[39] P.Castellini, M.Martarelli, E.P.Tomasini *Laser Doppler Vibrometry: Development of advanced solutions answering to technology's needs* Mechanical Systems and Signal Processing, Volume 20, Issue 6 (2006), 1265?1285

[40] A. Betzwar-Kotas *Größeneinfluss auf die mechanische Eigenschaften und das Wechselverformungsverhalten von dünnen Kupferfolien* Dissertation Universität Wien (2009)

[41] M.Aicheler *Influence of grain orientation on evolution of surface features in fatigued polycrystalline copper: a comparison of thermal and uniaxial mechanical fatigue results* Journal of Physics: Conference Series 240 (2010) 012051

[42] M. Aicheler, S. Sgobba, G. Arnau-Izquierdo, M. Taborelli, S. Calatroni, H. Neupert, W. Wuensch *Evolution of surface topography in dependence on the grain orientation during surface thermal fatigue of polycrystalline copper.* International Journal of Fatigue 33 (2011) 396?402

[43] S.P.Baker, A.Kretschmann, E.Arzt *Thermomechanical behaviour of different texture components in Cu thin films* Acta materialia 49 (2001) 2145-2160

[44] C. Rudolph *Untersuchung zum Einfluss von Additiven in Cu Plating Bädern auf die Kirkendall-Void Bildung.* Diploma thesis at the FH Regensburg, Regensburg (2010).

[45] N.L. Phung, V. Favier, N. Ranc, F. Valès, H. Mughrabi *Very high cycle fatigue of copper: Evolution, morphology and locations of surface slip markings* International journal of fatigue, volume 63 (2014) 68-77